

# 000 001 002 003 004 005 006 007 008 009 010 011 012 013 014 015 016 017 018 019 020 021 022 023 024 025 026 027 028 029 030 031 032 033 034 035 036 037 038 039 040 041 042 043 044 045 046 047 048 049 050 051 052 053 STABILIZING POLICY GRADIENTS FOR SAMPLE-EFFICIENT REINFORCEMENT LEARNING IN LLM REASONING

Anonymous authors

Paper under double-blind review

## ABSTRACT

Reinforcement Learning, particularly through policy gradient methods, has played a central role in enabling reasoning capabilities of Large Language Models. However, the optimization stability of policy gradients in this setting remains under-studied. As a result, existing implementations often resort to conservative hyper-parameter choices to ensure stability, which requires more training samples and increases computational costs. Hence, developing models for reliably tracking the underlying optimization dynamics and leveraging them into training enables more sample-efficient regimes and further unleashes scalable post-training. We address this gap by formalizing the stochastic optimization problem of policy gradients with explicit consideration of second-order geometry. We propose a tractable computational framework that tracks and leverages curvature information during policy updates. We further employ this framework to design interventions in the optimization process through data selection. The resultant algorithm, Curvature-Aware Policy Optimization (CAPO), identifies samples that contribute to unstable updates and masks them out. Theoretically, we establish monotonic improvement guarantees under realistic assumptions. On standard math reasoning benchmarks, we empirically show that CAPO ensures stable updates under aggressive learning regimes where baselines catastrophically fail. With minimal intervention (rejecting fewer than 8% of tokens), CAPO achieves up to 30 $\times$  improvement in sample efficiency over standard GRPO for LLM reasoning.

## 1 INTRODUCTION

The emergence of reasoning capabilities in Large Language Models (LLMs) represents a major shift in AI research. Beyond language understanding, reasoning has become a core ingredient of widely deployed systems (OpenAI et al., 2024; Gemini, 2025), enabling applications such as mathematical problem solving (Shao et al., 2024), code generation (Shojaee et al., 2023), and agentic workflows (Yao et al., 2023). This progress is primarily attributed to advances in scaling Reinforcement Learning (RL) techniques for LLM post-training, particularly policy gradient methods such as PPO (Schulman et al., 2017), GRPO (Shao et al., 2024), and variants (Yu et al., 2025; Liu et al., 2025b). These methods enabled LLMs to develop behaviors for autonomous chain-of-thought reasoning (Gandhi et al., 2025) and to effectively scale test-time compute (Setlur et al., 2025).

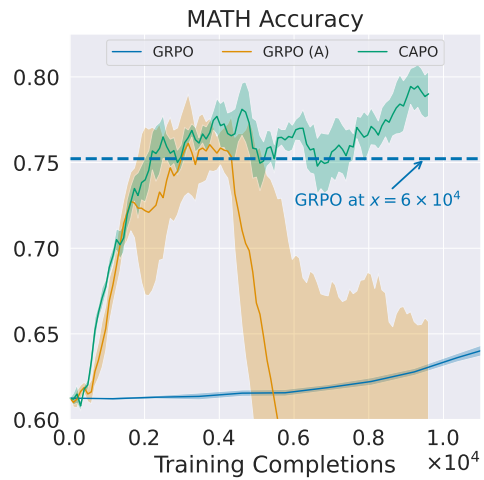


Figure 1: **Accuracy on MATH dataset from different RL methods.** CAPO (ours) achieves 30 $\times$  greater sample efficiency under an aggressive (A) update regime (higher learning rate, smaller batch size), whereas GRPO suffers policy collapse.

054 Despite its success in LLM fine-tuning and other decision-making tasks (Bellemare et al., 2020;  
 055 Mnih et al., 2015), RL still faces fundamental challenges that limit its broader practicality and  
 056 scalability. In particular, policy gradients suffer from optimization instabilities driven by the non-  
 057 stationary nature of the RL objective and the high variance of estimates (Castanyer et al., 2025).  
 058 These problems are further compounded by the known pathologies of training deep networks (Pas-  
 059 canu et al., 2013; Pennington et al., 2017). These factors lead to several undesired consequences,  
 060 such as catastrophic updates and policy collapse (Dohare et al., 2023), plasticity loss (Juliani & Ash,  
 061 2024), sample inefficiency (Kaiser et al., 2020), and hyperparameter sensitivity (Henderson et al.,  
 062 2018). As a result, the optimization dynamics of RL remain an active area of research from both  
 063 theoretical and empirical standpoints (Mei et al., 2022; Lyle et al., 2022; Vaswani et al., 2022).

064 Perhaps due to the recency of the topic, the optimization dynamics of RL *in the context of LLMs*  
 065 remains underexplored. These challenges persist in the LLM setting and may be even more pro-  
 066 nounced, since training involves billion-parameter models with very deep architectures and sam-  
 067 pling horizons that can extend arbitrarily. In practice, current implementations of RL for LLMs  
 068 typically rely on conservative hyperparameters to ensure stability, such as low learning rates (e.g.,  
 069  $3 \times 10^{-6}$  or less) and large batch sizes (e.g. thousands of generations per policy update) (Sheng  
 070 et al., 2024; Hugging Face, 2025; Guo et al., 2025). These choices substantially increase the number  
 071 of LLM generations required for learning, raising computational costs. Therefore, stabilizing these  
 072 algorithms in sample-efficient regimes is crucial to further scale RL for LLM reasoning.

073 One promising direction is to design algorithms that explicitly model second-order geometry in  
 074 the optimization landscape and incorporate this information into policy updates. In this work, we  
 075 formalize the RL optimization problem accounting for curvature terms, namely the Hessian of the  
 076 objective and the Fisher Information Matrix of the policy distribution. Building on this formulation,  
 077 we introduce a computationally and numerically tractable model of optimization dynamics that ap-  
 078 proximates this curvature information. This model enables continuous monitoring of gradient and  
 079 curvature estimates during policy updates, scales to billion-parameter models and provides analyti-  
 080 cal expressions for these quantities, which facilitate a systematic analysis of the learning dynamics.

081 We further leverage this optimization model to *plan* the next policy gradient step<sup>1</sup>. It allows *antic-*  
 082 *ipating* policy updates that potentially induce sudden shifts in the objective or policy distribution –  
 083 often associated with unstable optimization behavior – and intervening before taking the actual step  
 084 in the LLM. We propose a simple data selection mechanism as intervention: we identify particu-  
 085 lar samples that heavily contribute to these abrupt shifts and mask them out of the policy gradient  
 086 estimation. We refer to this method as *Curvature-Aware Policy Optimization* (CAPO).

087 We theoretically establish monotonic policy improvement guarantees under CAPO with practical  
 088 assumptions. We then empirically validate CAPO on standard math reasoning benchmarks, show-  
 089 ing that it yields stable optimization even in regimes with aggressive updates, where standard RL  
 090 algorithms suffer catastrophic updates and policy collapse. As a result, CAPO achieves up to 30×  
 091 improvement in sample efficiency [compared to GRPO in the standard regime](#), as presented in Figure 1. Lastly, we show that its interventions are minimal, typically rejecting fewer than 8% of the  
 092 tokens, with negligible computational overhead.

## 094 2 RELATED WORK

095 **RL & LLMs.** The use of RL techniques to optimize LLMs has been an active area of research  
 096 in recent years. Early work focused on RL from Human Feedback (RLHF), which optimizes poli-  
 097 cies toward modeled human preferences (Ziegler et al., 2019; Stiennon et al., 2020; Ouyang et al.,  
 098 2022). More recently, RL for LLM reasoning has gained significant attention for its effectiveness in  
 099 enabling autonomous chain-of-thought reasoning (Gandhi et al., 2025) and in scaling test-time com-  
 100 pute (Setlur et al., 2025). This breakthrough was initially driven by the seminal works of the OpenAI  
 101 o-series (OpenAI et al., 2024) and DeepSeek-R1 (Guo et al., 2025), which popularized GRPO (Shao  
 102 et al., 2024). Since then, the research community has studied several aspects of the training pipeline  
 103 (Zhang et al., 2025), including alternative objectives (Roux et al., 2025; Hu et al., 2025), sampling  
 104 mechanisms (Yu et al., 2025), reward shapings (Yang et al., 2024), and different training configura-  
 105

106 <sup>1</sup>In this work, “model” refers to the proposed computational model of curvatures and “policy” to the LLM.  
 107 “Model gradients” are computed under the former, while “policy gradients” denote the true LLM gradients.

108 tions (Liu et al., 2025b; Team et al., 2025). Our work fits within this line of research by investigating  
 109 RL for LLMs from an optimization dynamics perspective, proposing a model of the optimization  
 110 landscape and using it to design stable policy gradient updates.

111 **Optimization Dynamics in RL.** The non-convex and non-stationary nature of RL training has  
 112 motivated a large body of work on understanding and stabilizing optimization dynamics in RL agents.  
 113 In the context of policy gradients, prior research has investigated the role of baselines (Mei et al.,  
 114 2022), variance reduction techniques (Greensmith et al., 2001), and emergent pathologies such as  
 115 plasticity or capacity loss (Sokar et al., 2023; Klein et al., 2024) and policy collapse (Dohare et al.,  
 116 2023). Beyond these analyses, past literature has also developed conservative policy optimization  
 117 methods (Schulman et al., 2015; 2017; Achiam et al., 2017). While this line of work is exten-  
 118 sive and evolving, we primarily highlight the recent contribution of Castanyer et al., which, like  
 119 ours, examines the stabilization of policy gradients through curvature-informed interventions. Their  
 120 methodology, however, differs: they apply natural gradients with K-FAC (Eschenhagen et al., 2023)  
 121 in general deep RL environments, whereas our work develops a new approximation of curvature that  
 122 is tractable at the scale of LLMs and is incorporates it into optimization through data selection.

123 **Improving RL for LLM Reasoning.** In the context of LLM research, a nascent but growing litera-  
 124 ture explores improvements to RL training for reasoning. These works typically propose heuristics  
 125 that target specific problems observed during training—for example, noisy gradient estimates, lim-  
 126 ited output diversity, or large policy updates. Common approaches include rethinking advantage  
 127 estimation (Liu et al., 2025a; Ahmadian et al., 2024), controlling policy entropy (Yu et al., 2025;  
 128 Cui et al., 2025), and bounding advantage estimates or log-likelihoods Yang et al. (2025a;b). In  
 129 contrast, our work takes a more principled approach. Rather than introducing heuristics to address  
 130 isolated issues, we develop a framework based on second-order stochastic optimization that funda-  
 131 mentally explains these instabilities and addresses them in a unified manner.

### 132 3 PRELIMINARIES

133 **Problem Statement.** We formulate the problem of next-token generation as a Markov Decision  
 134 Process (MDP), defined by the tuple  $\mathcal{M} = (\mathcal{S}, \mathcal{A}, \mathcal{P}, R, \rho_0, \gamma, T)$ , in which  $\mathcal{S}$  is a state space,  $\mathcal{A}$   
 135 is an action space,  $\mathcal{P} : \mathcal{S} \times \mathcal{A} \rightarrow \Delta(\mathcal{S})$  a transition function,  $R : \mathcal{S} \times \mathcal{A} \rightarrow [-r_{\text{bound}}, +r_{\text{bound}}]$  a  
 136 bounded reward function,  $\rho_0 : \mathcal{S} \rightarrow \Delta(\mathcal{S})$  an initial state distribution,  $\gamma \in [0, 1]$  a discount factor,  
 137 and  $T$  the length of the horizon. In the LLM setting, let  $\mathcal{V}$  be a token vocabulary and  $L \in \mathbb{N}$  a  
 138 maximum sequence length, including both prompt and generated tokens.  $\mathcal{S} = \bigcup_{n=0}^L \mathcal{V}^n$  is the set  
 139 of all finite sequences, with each state  $s_t \in \mathcal{S}$  representing the concatenation of the prompt and  
 140 the tokens generated up to time  $t$ , with total length at most  $L$ .  $\mathcal{A}$  is the space spanned by  $\mathcal{V}$ : at  
 141 each step, the policy selects a token  $a_t \in \mathcal{V}$ .  $\mathcal{P}$  is governed by autoregressive sampling and takes  
 142 the form of a trivial deterministic function  $s_{t+1} = s_t \circ a_t$ , where  $\circ$  denotes concatenation. The  
 143 initial state distribution  $\rho_0$  specifies a distribution over prompts. During policy optimization, one  
 144 typically optimizes a parameterized LLM  $\pi_{\theta} : \mathcal{S} \times \mathcal{A} \rightarrow \Delta(\mathcal{A})$ , with the objective of maximizing  
 145 the expected cumulative reward over the generated sequence:

$$146 J(\theta) = \mathbb{E}_{\tau \sim \pi_{\theta}} \left[ \sum_{t=0}^T \gamma^t R(s_t, a_t) \right], \quad (1)$$

147 where  $\tau$  denotes a trajectory,  $s_0 \sim \rho_0(s_0)$ ,  $a_t \sim \pi_{\theta}(a_t | s_t)$ , and  $s_{t+1} = s_t \circ a_t$ .

148 **Policy Gradient (PG)** methods optimize a stochastic policy by differentiating  $J(\theta)$  with respect to  
 149 the policy parameters (Williams, 1992) and can be written as (Sutton et al., 1999):

$$150 \nabla_{\theta} J(\theta) = \mathbb{E}_{\tau \sim \pi_{\theta}} \left[ \sum_{t=0}^T \gamma^t \nabla_{\theta} \log \pi_{\theta}(a_t | s_t) R(s_t, a_t) \right]. \quad (2)$$

151 This expectation can be estimated via Monte Carlo sampling under the current policy  $\pi_{\theta}$ . However,  
 152 such estimates often have high variance. A standard remedy is to subtract a baseline  $b(s_t)$  which  
 153 leaves the gradient unbiased while reducing variance. In practice, this is typically done by replacing  
 154 the reward with an estimate of the advantage function  $A(s_t, a_t)$ . For the rest of this work, we will  
 155 assume the advantage version of this objective.

162 **Group Relative Policy Optimization** (Shao et al., 2024) is a widely used method for RL in LLMs.  
 163 Akin to PPO (Schulman et al., 2017), it optimizes a surrogate objective that employs off-policy  
 164 correction Kakade & Langford (2002) with a clipping strategy to prevent large deviations:  
 165

$$166 \quad J_{\text{GRPO}}(\boldsymbol{\theta}) = \mathbb{E}_{\tau \sim \pi_{\beta}} \left[ \frac{1}{|\tau_i|} \sum_{t=0}^{|\tau_i|} \min \left( r_{\theta}(s_t, a_t), \text{clip}(r_{\theta}(s_t, a_t), 1 - \epsilon, 1 + \epsilon) \right) A^{\text{GRPO}}(s_t, a_t) \right. \\ 167 \quad \left. - \beta \mathcal{D}_{\text{KL}}(\pi_{\theta}(\cdot | s_t) \| \pi_{\text{base}}(\cdot | s_t)) \right], \quad (3)$$

170 where  $r_{\theta}(s_t, a_t) = \frac{\pi_{\theta}(a_t | s_t)}{\pi_{\beta}(a_t | s_t)}$  and  $\pi_{\beta}$  is the sampling policy. The KL divergence term acts as a regularizer that penalizes deviation from  $\pi_{\text{base}}$ , the initial LLM. In contrast to standard PG methods, GRPO draws samples in groups: for each prompt  $s_0 \sim \rho_0(s_0)$ , it generates a group of trajectories  $\{\tau_i\}_{i=1}^G \sim \pi_{\beta}$ . Contributions from all state-action pairs of a trajectory are averaged (rather than discounted), which effectively assume  $\gamma = 1$  with per-trajectory normalization. Finally, the advantage estimator is defined as:  
 171  
 172  
 173  
 174  
 175

$$177 \quad \hat{A}^{\text{GRPO}}(s_t, a_t) = \frac{\hat{R}(\tau) - \bar{R}}{\hat{\sigma}_R + \varepsilon}, \quad \bar{R} = \frac{1}{G} \sum_{i=1}^G \hat{R}(\tau_i), \quad \hat{\sigma}_R = \sqrt{\frac{1}{G} \sum_{i=1}^G (\hat{R}(\tau_i) - \bar{R})^2}, \quad (4)$$

180 where  $\hat{R}(\tau)$  is the return for trajectory  $\tau$  and  $\varepsilon$  is a small constant for numerical stability.  
 181

## 182 4 MODELING THE OPTIMIZATION LANDSCAPE WITH SECOND-ORDER 183 GEOMETRY

186 In this section, we develop a model of the optimization landscape. We formulate the reinforcement  
 187 learning (RL) optimization problem with policy gradients by explicitly incorporating second-order  
 188 geometric information. Building on this formulation, we introduce a tractable computational model  
 189 that approximates the role of curvature during learning. Our hypothesis is that by providing a simple  
 190 but effective approximation of second-order gradients, one could track sudden shifts in the objective  
 191 or policy and anticipate potentially unstable updates.

192 **The Higher-Order Objective.** Consider the objective function  $J(\boldsymbol{\theta})$  as in Equation 1. After an  
 193 update step  $\Delta\boldsymbol{\theta}$ , the new objective  $J(\boldsymbol{\theta} + \Delta\boldsymbol{\theta})$  is given by the following Taylor expansion:

$$194 \quad J(\boldsymbol{\theta} + \Delta\boldsymbol{\theta}) = J(\boldsymbol{\theta}) + \underbrace{\nabla_{\boldsymbol{\theta}} J(\boldsymbol{\theta})^{\top} \Delta\boldsymbol{\theta} + \frac{1}{2} \Delta\boldsymbol{\theta}^{\top} H(\boldsymbol{\theta}) \Delta\boldsymbol{\theta}}_{m_H(\Delta\boldsymbol{\theta})} + \mathcal{O}(\|\Delta\boldsymbol{\theta}\|^3), \quad (5)$$

197 where  $H(\boldsymbol{\theta})$  denotes the Hessian of the objective. Equation 5 holds under a Lipschitz continuous  
 198 Hessian (see Assumption A.1), with a detailed proof in Appendix A. As the cubic term may be  
 199 negative, we can establish a guaranteed lower bound  $J(\boldsymbol{\theta} + \Delta\boldsymbol{\theta}) \geq J(\boldsymbol{\theta}) + m_H(\Delta\boldsymbol{\theta}) - \mathcal{O}(\|\Delta\boldsymbol{\theta}\|^3)$ .  
 200 In practice, the cubic term is often negligible, and we approximate the objective change by  $m_H(\Delta\boldsymbol{\theta})$ .  
 201 Crucially, standard gradient ascent ignores the Hessian contribution, which can lead to a decrease in  
 202 the objective for non-convex problems (such as RL) when this contribution is sufficiently negative.  
 203

204 **The Fisher Information Matrix.** The Hessian captures the local curvature of the objective function.  
 205 In RL, however, the objective is non-stationary, and what ultimately matters is how updates  
 206 change the policy distribution. For instance, an update may produce only a small change in the  
 207 objective while inducing a large shift in the policy. This alters how future trajectories are sampled  
 208 and may destabilize learning. Therefore, it is necessary to track the geometry of the policy distribution  
 209 directly, which is what the Fisher Information Matrix (FIM) enables. One can show that the  
 210 directional curvature under the Fisher geometry approximates the average KL divergence between a  
 211 policy and before and after a small step  $\Delta\boldsymbol{\theta}$ :

$$211 \quad \bar{D}_{\text{KL}}(\pi_{\boldsymbol{\theta}} \| \pi_{\boldsymbol{\theta} + \Delta\boldsymbol{\theta}}) = \underbrace{\frac{1}{2} \Delta\boldsymbol{\theta}^{\top} F(\boldsymbol{\theta}) \Delta\boldsymbol{\theta}}_{m_F(\Delta\boldsymbol{\theta})} + \mathcal{O}(\|\Delta\boldsymbol{\theta}\|^3), \quad (6)$$

214 where  $\bar{D}_{\text{KL}}(\pi_{\boldsymbol{\theta}} \| \pi_{\boldsymbol{\theta} + \Delta\boldsymbol{\theta}}) := \mathbb{E}_{s \sim d_{\pi}} [\text{KL}(\pi_{\boldsymbol{\theta}}(\cdot | s) \| \pi_{\boldsymbol{\theta} + \Delta\boldsymbol{\theta}}(\cdot | s))]$ , and  $F(\boldsymbol{\theta}) :=$   
 215  $\mathbb{E}_{s \sim d_{\pi}, a \sim \pi_{\boldsymbol{\theta}}(\cdot | s)} [\nabla_{\boldsymbol{\theta}} \log \pi_{\boldsymbol{\theta}}(a | s) \nabla_{\boldsymbol{\theta}} \log \pi_{\boldsymbol{\theta}}(a | s)^{\top}]$  is the FIM. The proof is in Appendix

216 B. Similarly to the Hessian case, the cubic term is often negligible and we focus on  $m_F(\Delta\theta)$ . One  
 217 can further show that enforcing a trust region  $\bar{D}_{\text{KL}}(\pi_\theta \parallel \pi_{\theta+\Delta\theta}) \leq \delta$  during policy updates leads to  
 218 monotonic improvement of the true objective, given sufficiently small  $\delta$  (Schulman et al., 2015).

219 Ultimately, we aim to design a model that approximates  $m_H(\Delta\theta)$  and  $m_F(\Delta\theta)$  without explicitly  
 220 computing gradients or curvature terms in the high-dimensional parameter space of the LLM. This  
 221 approach can be viewed as a form of model-based RL, but from a different perspective: whereas  
 222 prior work typically models components of the MDP, such as the dynamics or reward function, we  
 223 instead model the optimization process itself, which allows us to plan gradient estimates.

#### 225 4.1 COMPUTATIONAL MODEL

227 For an LLM with  $d$  parameters, both Hessian and FIM are  $d \times d$  matrices, which is intractable  
 228 for billion-size parameter spaces. Even approximations such as K-FAC (Eschenhagen et al., 2023)  
 229 would incur unfeasible memory cost. Therefore, we need to devise a computational model that  
 230 is scalable and effectively provides curvature information to stabilize policy gradients. Next, we  
 231 describe our methodology.

232 **Last-Layer Model.** Since modeling the full Hessian or Fisher Information Matrix (FIM) is in-  
 233 feasible, we restrict attention to curvature in a parameter subspace. To this end, we adopt a sim-  
 234 ple last-layer approach. An LLM is a softmax policy over the token vocabulary  $\pi_\theta(a \mid s) =$   
 235  $\frac{\exp(f_\theta(s, a))}{\sum_{a'} \exp(f_\theta(s, a'))}$ , where  $f_\theta(s, a) \in \mathbb{R}$  are the logits produced by the network. Letting  $f_\theta(s_t)$  denote  
 236 the full logits vector, with  $\theta = (\bar{\theta}, \psi)$ , we represent the pre-softmax layer as  $f_\theta(s_t) = Wh_{\bar{\theta}}(s_t)$ ,  
 237 where  $W \in \mathbb{R}^{K \times d_i}$  is the last-layer weight matrix,  $K = \dim(\mathcal{V})$ , and  $h_{\bar{\theta}}(s_t) \in \mathbb{R}^{d_i}$ . We then define  
 238  $\psi = \text{vec}(W) \in \mathbb{R}^{K \cdot d_i}$ . In Appendix C, we show that the last-layer model gradient  $\tilde{g}(\psi)$  of the  
 239 objective in Equation 1 is:

$$241 \tilde{g}(\psi) = \mathbb{E}_{\tau \sim \pi_\theta} \left[ \sum_{t=0}^T \gamma^t A(s_t, a_t) (e_a - \pi_\theta(s_t)) \otimes h_{\bar{\theta}}(s_t) \right], \quad (7)$$

244 where  $\otimes$  denotes a Kronecker product,  $e_{a_t} \in \mathcal{V}$  is the one-hot action vector  $e_{a_t} = \mathbf{1}\{a = a_t\}$ ,  
 245 and  $\pi_\theta(s_t)$  the policy distribution vector. We use the vectorization operation  $\text{vec}(\cdot)$  only for conve-  
 246 nience and it does not introduce new assumptions. In this work, we use a tilde superscript to denote  
 247 *model-based* gradients and curvatures, in contrast to the actual *policy* gradient  $g(\theta) := \nabla_\theta J(\theta)$ .

248 Under the last-layer model, the Hessian of the objective takes the following form:

$$250 \tilde{H}(\psi) = \mathbb{E}_{\tau \sim \pi_\theta} \left[ \sum_{t=0}^T \gamma^t A(s, a) \left( (e_a - \pi_\theta(s_t)) (e_a - \pi_\theta(s_t))^\top - F(s_t) \right) \otimes h_{\bar{\theta}}(s_t) h_{\bar{\theta}}(s_t)^\top \right], \quad (8)$$

253 where  $F(s_t)$  is the FIM for state  $s_t$ . In Lemma C.1, we show that this expression can be estimated  
 254 via samples. Similarly, the last-layer approximation of the FIM is:

$$255 \tilde{F}(\psi) = \mathbb{E}_{\tau \sim \pi_\theta} [((e_{a_t} - \pi_\theta(s_t)) (e_{a_t} - \pi_\theta(s_t))^\top) \otimes h_{\bar{\theta}}(s_t) h_{\bar{\theta}}(s_t)^\top]. \quad (9)$$

257 **Computing Directional Curvatures.** Even with the approximated model, the curvature matrices  
 258 have dimension  $Kd_i \times Kd_i$ . For current LLMs, where  $K > 10^5$  and  $d_i > 10^3$ , fully materializing  
 259 these matrices is computationally infeasible. Fortunately, our goal is to approximate the shifts in the  
 260 objective and policy,  $m_H(\Delta\theta)$  and  $m_F(\Delta\theta)$ . Thus, we only need to approximate the *directional*  
 261 curvatures  $\Delta\theta^\top C(\theta) \Delta\theta$ , without explicitly materializing the full Hessian or FIM. In Appendix  
 262 D, we present a mechanism that enables this computation without constructing large tensors. Our  
 263 method requires storing only  $\mathcal{O}(Kd_i)$  tensors per state-action sample, instead of the  $\mathcal{O}((Kd_i)^2)$   
 264 entries of the full curvature matrices.

265 **Exploiting Gradient Sparsity.** We further reduce complexity by exploiting the structure of gradi-  
 266 ents arising from LLM generation. Standard LLM decoding relies on selective sampling methods  
 267 (e.g., top-k, nucleus sampling) Wolf et al. (2020) to improve generation quality, as most of the prob-  
 268 ability mass is concentrated on a small subset  $k$  of the vocabulary (Fan et al., 2018; Holtzman et al.,  
 269 2020), typically with  $k < 100$ . Consequently, only  $k$  tokens have non-zero probability at each genera-  
 270 tion step, which implies that only the  $k \cdot d_i$  parameters of the last-layer weight matrix  $W$  associated

270 with these logits yield non-zero gradients. We therefore store and operate these gradients in sparse  
 271 form. This sparsity also applies to the computation of directional curvatures in Equations 58 and 63,  
 272 as these reduce to dot products involving sparse vectors (e.g.,  $(e_{a_t} - \pi_\theta(s_t)$  and the model-based  
 273 update step  $\Delta\theta$ ). Naturally, as we estimate gradients with more samples, the representation expands  
 274 to cover all  $\tilde{k}$  tokens generated, but typically  $\tilde{k} \ll K$ . For instance, our experiments presented  
 275  $\tilde{k} < 10^4$ . Overall, the memory and dot product complexity reduce to  $\mathcal{O}(\tilde{k} \cdot d_i)$ .

276 **Modeling the Step  $\Delta\theta$ .** A final design choice concerns how to model the planned update steps,  
 277  $\Delta\theta$ . Under the last-layer model, these steps take the form  $\Delta\psi$ . This choice essentially determines  
 278 how we represent the optimizer. A simple option is to model the update as a stochastic gradient  
 279 descent (SGD) step,  $\Delta\psi = \alpha\tilde{g}$ , where  $\alpha$  is the learning rate. Alternatively, we can match the LLM  
 280 optimizer, which in our case is Adam (Kingma & Ba, 2015), i.e.,  $\Delta\psi = \alpha\frac{\hat{p}_t}{\sqrt{\hat{q}_t + \epsilon}}$ , where  $\hat{p}_t$  and  $\hat{q}_t$   
 281 are the bias-corrected first and second moment estimates of the gradient.

## 283 5 CURVATURE-AWARE POLICY OPTIMIZATION

284 We may now compute the objective and policy shifts under our model as:

$$285 \quad m_H(\psi) = \tilde{g}(\psi)^\top \Delta\psi + \frac{1}{2} \Delta\psi^\top \tilde{H}(\psi) \Delta\psi, \quad m_F(\psi) = \frac{1}{2} \Delta\psi^\top \tilde{F}(\psi) \Delta\psi, \quad (10)$$

286 and estimate  $m_H$  and  $m_F$  via samples following the methodology described in the subsection 4.1.  
 287 We now design an algorithm that intervenes in the optimization of the underlying LLM policy using  
 288 the model-based updates. Since our objective is to stabilize policy gradients in sample-efficient  
 289 regimes, a natural choice is to construct an algorithm that follows the principles of trust-region  
 290 methods (Murphy, 2022). We implement this idea through a rejection sampling mechanism.

291 Given a batch  $\mathcal{B}$  of collected trajectories, we partition it into disjoint subsets  $b_i \subset \mathcal{B}$ . For each  
 292 subset, we compute a proposed step  $\Delta\psi_i$  and evaluate the shifts defined in Equation 10. We then  
 293 accept a subset if it satisfies the (local) trust-region constraints  $\delta_F$ ,  $\delta_H$ , and  $\delta_H^{high}$ :

$$294 \quad \delta_H \leq m_H(\Delta\psi_i) \leq \delta_H^{high}, \quad m_F(\Delta\psi_i) \leq \delta_F. \quad (11)$$

295 The accepted subsets are subsequently used to compute the gradient update of the LLM policy. Conceptually, this mechanism is analogous to token masking. Overall, this data selection mechanism is  
 296 simple, computationally inexpensive, and flexible, as it can be applied at different granularities, including tokens, sentences, groups, or full batches. The formal pseudocode is provided in Algorithm  
 297 1. Next, we establish theoretical results for monotonic policy improvement under CAPO.

298 **Theorem 5.1** (Monotonic improvement under CAPO). *Fix thresholds  $\delta_H > 0$  and  $\delta_F > 0$ . Let  $\mathcal{B}$   
 299 be a batch of sampled trajectories. Split  $\mathcal{B}$  into disjoint  $N$  subsets  $b_i \subset \mathcal{B}$ , and propose candidate  
 300 subset updates  $\{\Delta\theta_i\}_{i:N}$ . Retain those satisfying:*

$$301 \quad m_H(\Delta\theta_i) \geq \delta_H = \omega + \frac{1}{2}Mr^2, \quad m_F(\Delta\theta_i) \leq \delta_F, \quad (12)$$

302 with  $\omega > 0$  and  $M, r$  defined as in Assumption E.1. Let  $\mathcal{B}_{acc}$  denote the superset of the  $\mathcal{B}$  accepted  
 303 subsets, and define the aggregated update:  $\Delta\theta = \frac{1}{B} \sum_{i \in \mathcal{B}_{acc}} \Delta\theta_i$ . Then, for two policies  $\pi_\theta$  and  
 304  $\pi_{\theta+\Delta\theta}$ , with  $|A^\pi(s, a)| \leq \epsilon$ , we obtain:

$$305 \quad J(\pi_{\theta+\Delta\theta}) - J(\pi_\theta) \geq \omega - C\sqrt{\delta_F}, \quad C = \frac{2\gamma}{(1-\gamma)^2} \epsilon \sqrt{2}. \quad (13)$$

306 Thus choosing  $\omega \geq C\sqrt{\delta_F}$  guarantees monotonic improvement:  $J(\pi_{\theta+\Delta\theta}) \geq J(\pi_\theta)$ .

307 The proof is provided in Appendix E. Observe that  $\delta_H^{high}$  is not required to establish monotonic  
 308 improvement. Nonetheless, it serves as a safeguard against overly aggressive steps. In practice,  
 309 introducing this upper cap reduces the observed  $M$  and  $r$ , which allows the use of smaller  $\delta_H$ .  
 310 Finally, we note that Theorem 5.1 relies on the true objective and policy shifts, whereas in practice  
 311 these quantities are approximated using our model.

## 321 6 EXPERIMENTS AND DISCUSSION

322 In this section, we evaluate (i) how the proposed computational model captures the optimization  
 323 landscape, and (ii) how this information can be used to stabilize RL optimization dynamics through

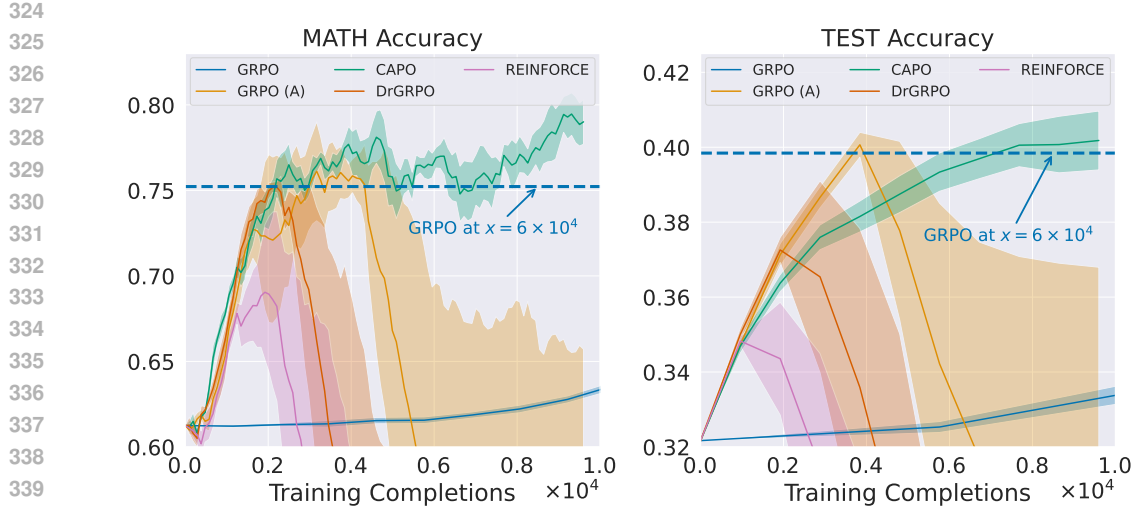


Figure 2: **Comparison with baseline methods on policy gradient stability.** While the setup with more aggressive updates makes all methods more sample-efficient, it also leads the baselines to policy collapse. In contrast, CAPO prevents collapse and achieves up to 30× greater sample efficiency than GRPO under aggressive updates.

CAPO. Our central hypothesis is that an inexpensive yet effective approximation of second-order geometry can track unstable shifts in the objective and policy, and that this information can in turn be used to stabilize aggressive update regimes, leading to more sample-efficient RL in LLMs.

**Experimental Setup.** We consider a standard RL setup for finetuning LLMs on reasoning tasks. Our implementation builds on the Open-R1 open-source project (Hugging Face, 2025), and we maximize an accuracy-based reward. Following prior work, we fine-tune a Qwen2.5-Math-7B LLM (Qwen et al., 2025) on mathematical reasoning questions. Our primary evaluation metric is accuracy, but we also track optimization-related quantities such as gradient and curvature statistics and token rejection rates. Since our goal is to evaluate sample efficiency, we report all metrics as a function of the number of training completions (i.e., LLM *trajectories* generated). Appendix G provides additional details regarding implementation, hyperparameters, and compute resources<sup>2</sup>.

**Datasets & Benchmarks.** We train our policies on the MATH dataset (Hendrycks et al., 2021). For evaluation, we consider eight benchmarks: GSM8K (Cobbe et al., 2021), MATH500 (Lightman et al., 2023), OlympiadBench (He et al., 2024), MinervaMath (Lewkowycz et al., 2022), GPQA:Diamond (Rein et al., 2023), AMC23, AIME24, and AIME25. Most of these benchmarks contain mathematical questions at varying levels (high school, graduate, and olympiad), while GPQA focuses on general STEM-related problems. For simplicity, we report the average performance across all eight benchmarks, which we refer to as “TEST” in the results.

**Comparison Methods.** We evaluate our approach against two GRPO variants. The first corresponds to the standard “conservative” update regime implemented in the Open-R1 codebase. The second, which we denote “GRPO (A),” adopts a more aggressive regime intended to improve sample efficiency, with a learning rate 5× higher and a batch size 12× smaller. This matches the configuration used by CAPO. We also evaluate Dr.GRPO (Liu et al., 2025a) and REINFORCE (Williams, 1992), both under the same aggressive regime.

**CAPO operationalization.** CAPO optimizes the same objective as GRPO, but leverages the data selection mechanism introduced in Section 5. For a fair comparison, we use the same hyperparameters as GRPO (A). We implement CAPO with token-level selection, i.e., proposing steps  $\Delta\psi_i$  and rejecting samples on a per-token basis. Finally, we model optimization steps using Adam.

## 6.1 EXPERIMENTS

We highlight and analyze the following questions to evaluate our hypothesis and proposed method:

<sup>2</sup>We release our code at <https://anonymous.4open.science/r/capo-stable-gradients>.

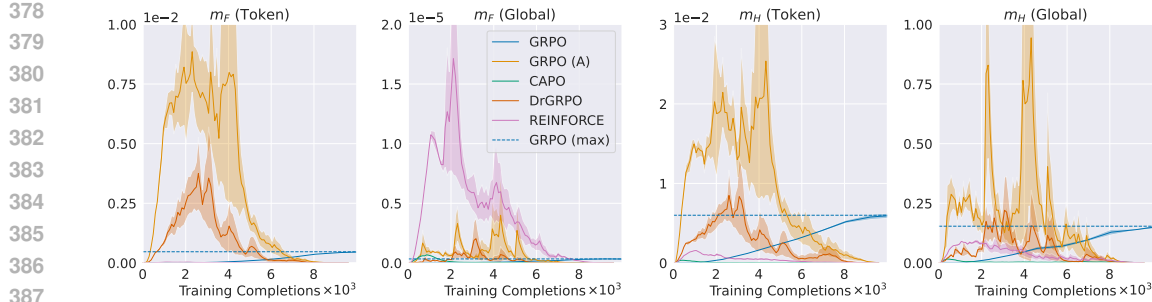


Figure 3: **Evaluation of policy and objective shifts estimates from the proposed computational model during training.** Unstable methods exhibit large and abrupt directional curvatures, while stable ones maintain much smaller and smoother shifts. CAPO, by applying token-level bounds, also ensures well-behaved shifts at the global (batch) level, supporting the rationale of Theorem 5.1.

**Does CAPO prevent instability in LLM policy gradients? Does it lead to better sample efficiency?** Figure 2 reports accuracy for all methods on MATH and on the TEST benchmark set. First, we observe that the more aggressive setup does lead to more sample-efficient learning than the conservative one across all methods. However, for the baselines, this improvement comes at the cost of stability. Under the aggressive regime, all baseline methods suffer from policy collapse, with performance dropping well below that of the base model and therefore losing the ability to learn further. In contrast, CAPO maintains stable performance throughout training, remaining effective long after all other methods have collapsed. This demonstrates that CAPO effectively prevents instability under aggressive updates. As a result, CAPO requires  $30\times$  fewer completions on MATH and  $9\times$  fewer completions on TEST compared to standard conservative GRPO.

**What does the proposed computational model reveal about the optimization landscape?** To analyze this question, we examine the policy shift  $m_F$  and the objective shift  $m_H$  at both the token level and the global (batch) level over the course of training, presented in Figure 3. For  $m_F$ , we find that unstable methods (GRPO (A), DrGRPO, REINFORCE) exhibit very high global directional curvatures during training, whereas stable methods (CAPO, standard GRPO) maintain much smaller shifts. In particular, the global  $m_F$  correlates closely with the instability observed in Figure 1, showing that the model, despite its simplicity, remains informative about optimization dynamics.

For  $m_H$ , we observe similar trends: unstable methods show abrupt shifts, while stable ones produce smoother, better-behaved curves. Note that, while a higher  $m_F$  directly signals instability since it tracks policy shifts, a higher  $m_H$  does not necessarily directly imply instability. This is because  $m_H$  depends on the adopted advantage function (Equation 37) and the normalization strategy of each method. Still, sharp peaks in the  $m_H$  curves also correlate with training instabilities. Lastly, we highlight that CAPO, by applying a local bound per token, also ensures well-behaved shifts at the global level, which supports the rationale of Theorem 5.1. Overall, these results highlight that the computational model provides meaningful information about the optimization landscape, and that CAPO effectively leverages this information to stabilize training.

**Can we extend curvature-aware selection to other RL methods?** To test this, we extend Dr.GRPO and REINFORCE by incorporating our proposed curvature-aware selection, resulting in Dr.CAPO and ReinCAPO, respectively. Figure 4 reports the evaluation results for these methods. In all cases, incorporating the selection strategy improves upon the base method and prevents policy collapse. These findings suggest that the proposed computational model and intervention mechanism are broadly applicable across different policy optimization objectives.

**How aggressive is CAPO’s intervention to ensure stability?** We analyze the extent of token rejection required by CAPO to maintain stable gradients, measured by the token rejection rate during training (Figure 5). The rejection rate peaks at about 8% in the early stages of opti-



Figure 5: **Token rejection rate under CAPO.** It maintains a low rejection rate over training, stabilizing learning with minimal intervention.

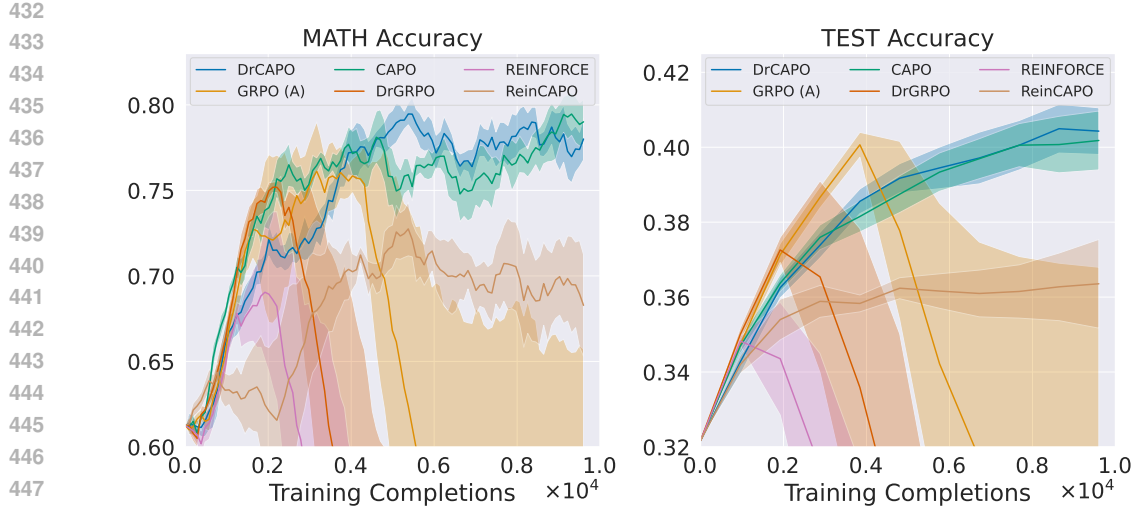


Figure 4: **Evaluation of extended versions of RL methods with curvature-aware selection.** Incorporating curvature-aware selection consistently improves the base methods, preventing policy collapse and demonstrating the broader applicability of our approach across different policy optimization objectives.

mization, when higher learning rates produce more aggressive updates, but quickly decreases and remains below 2% for the remainder of training. Overall, this shows that CAPO guides optimization toward stable curvature regions while keeping its intervention minimal, allowing the LLM to continue leveraging the vast majority of samples.

**Additional Experiments.** We provide a computational cost analysis of CAPO in Appendix H, where we show that the additional components incur minor overhead. Additionally, we present further experiments in Appendix I, including an ablation study on the optimizer model and a detailed evaluation of other heuristics traditionally used to ensure stability (e.g., PPO clipping and KL regularization), highlighting their limitations in the LLM setup.

## 7 FINAL REMARKS

In this work, we propose a computational framework that models curvature information and integrates it into policy updates through CAPO. We provide theoretical guarantees for CAPO and show that it is effective at identifying samples that contribute to unstable updates, preventing policy collapse in aggressive training regimes where standard RL methods for LLM reasoning fail. As a result, CAPO achieves up to a  $30\times$  improvement in sample efficiency compared to widely used training setups, while requiring only minimal intervention and computational overhead. Overall, it enables more sample-efficient learning regimes, supporting further scalability post-training scalability.

**Limitations.** Despite the encouraging results, we acknowledge some limitations of our work. First, due to compute budget constraints, we focused on experiments at a smaller, academic scale. While we demonstrated the effectiveness of CAPO against commonly used RL methods, future work could extend these results to distinct problem settings and longer training schedules. Second, the choice of CAPO thresholds depends on the problem setting (MDP, objective function, base policy) and may require tuning across different scenarios. Nonetheless, this is not a major concern, as the thresholds can be tuned solely on the training distribution.

**Future Work.** Beyond scalability, future research may explore different parametrizations of the computational model (for instance, by extending it to deeper layers) and investigate their impact on computational tractability and curvature estimates. In addition, future work may evaluate CAPO extensions to other intervention mechanisms, such as soft masking or regularization methods.

486 REFERENCES  
487

488 Joshua Achiam, David Held, Aviv Tamar, and Pieter Abbeel. Constrained policy optimization. In  
489 Doina Precup and Yee Whye Teh (eds.), *Proceedings of the 34th International Conference on  
490 Machine Learning*, volume 70 of *Proceedings of Machine Learning Research*, pp. 22–31. PMLR,  
491 06–11 Aug 2017. URL <https://proceedings.mlr.press/v70/achiam17a.html>.

492 Arash Ahmadian, Chris Cremer, Matthias Gallé, Marzieh Fadaee, Julia Kreutzer, Olivier Pietquin,  
493 Ahmet Üstün, and Sara Hooker. Back to basics: Revisiting REINFORCE-style optimization  
494 for learning from human feedback in LLMs. In Lun-Wei Ku, Andre Martins, and Vivek  
495 Srikumar (eds.), *Proceedings of the 62nd Annual Meeting of the Association for Compu-  
496 tational Linguistics (Volume 1: Long Papers)*, pp. 12248–12267, Bangkok, Thailand, August  
497 2024. Association for Computational Linguistics. doi: 10.18653/v1/2024.acl-long.662. URL  
498 <https://aclanthology.org/2024.acl-long.662/>.

499 S. Amari, A. Cichocki, and H. H. Yang. A new learning algorithm for blind signal separation.  
500 In *Proceedings of the 9th International Conference on Neural Information Processing Systems*,  
501 NIPS’95, pp. 757–763, Cambridge, MA, USA, 1995. MIT Press.

502 Shun-ichi Amari. Natural gradient works efficiently in learning. *Neural Computation*, 10(2):251–  
503 276, 1998. doi: 10.1162/089976698300017746.

504 Marc Bellemare, Salvatore Candido, Pablo Castro, Jun Gong, Marlos Machado, Subhodeep Moitra,  
505 Sameera Ponda, and Ziyu Wang. Autonomous navigation of stratospheric balloons using rein-  
506 force learning. *Nature*, 588:77–82, 12 2020. doi: 10.1038/s41586-020-2939-8.

507 Lukas Biewald. Experiment tracking with weights and biases, 2020. URL <https://www.wandb.com/>. Software available from wandb.com.

508 Roger Creus Castanyer, Johan Obando-Ceron, Lu Li, Pierre-Luc Bacon, Glen Berseth, Aaron  
509 Courville, and Pablo Samuel Castro. Stable gradients for stable learning at scale in deep rein-  
510 force learning, 2025. URL <https://arxiv.org/abs/2506.15544>.

511 Karl Cobbe, Vineet Kosaraju, Mohammad Bavarian, Mark Chen, Heewoo Jun, Lukasz Kaiser,  
512 Matthias Plappert, Jerry Tworek, Jacob Hilton, Reiichiro Nakano, Christopher Hesse, and John  
513 Schulman. Training verifiers to solve math word problems. *arXiv preprint arXiv:2110.14168*,  
514 2021.

515 Ganqu Cui, Yuchen Zhang, Jiacheng Chen, Lifan Yuan, Zhi Wang, Yuxin Zuo, Haozhan Li, Yuchen  
516 Fan, Huayu Chen, Weize Chen, Zhiyuan Liu, Hao Peng, Lei Bai, Wanli Ouyang, Yu Cheng,  
517 Bowen Zhou, and Ning Ding. The entropy mechanism of reinforcement learning for reasoning  
518 language models, 2025. URL <https://arxiv.org/abs/2505.22617>.

519 Shibhansh Dohare, Qingfeng Lan, and A. Rupam Mahmood. Overcoming policy collapse in deep  
520 reinforcement learning. In *Sixteenth European Workshop on Reinforcement Learning*, 2023. URL  
521 <https://openreview.net/forum?id=m9Jfdz4ymO>.

522 Runa Eschenhagen, Alexander Immer, Richard Turner, Frank Schneider, and Philipp Hennig.  
523 Kronecker-factored approximate curvature for modern neural network architectures. In A. Oh,  
524 T. Naumann, A. Globerson, K. Saenko, M. Hardt, and S. Levine (eds.), *Advances in Neu-  
525 ral Information Processing Systems*, volume 36, pp. 33624–33655. Curran Associates, Inc.,  
526 2023. URL [https://proceedings.neurips.cc/paper\\_files/paper/2023/file/6a6679e3d5b9f7d5f09cdb79a5fc3fd8-Paper-Conference.pdf](https://proceedings.neurips.cc/paper_files/paper/2023/file/6a6679e3d5b9f7d5f09cdb79a5fc3fd8-Paper-Conference.pdf).

527 Angela Fan, Mike Lewis, and Yann Dauphin. Hierarchical neural story generation. In Iryna  
528 Gurevych and Yusuke Miyao (eds.), *Proceedings of the 56th Annual Meeting of the Associa-  
529 tion for Computational Linguistics (Volume 1: Long Papers)*, pp. 889–898, Melbourne, Aus-  
530 tralia, July 2018. Association for Computational Linguistics. doi: 10.18653/v1/P18-1082. URL  
531 <https://aclanthology.org/P18-1082/>.

532 Kanishk Gandhi, Ayush Chakravarthy, Anikait Singh, Nathan Lile, and Noah D. Goodman. Cogni-  
533 tive behaviors that enable self-improving reasoners, or, four habits of highly effective stars, 2025.  
534 URL <https://arxiv.org/abs/2503.01307>.

540 Gemini. Gemini 2.5: Pushing the frontier with advanced reasoning, multimodality, long context, and  
 541 next generation agentic capabilities, 2025. URL <https://arxiv.org/abs/2507.06261>.

542

543 Evan Greensmith, Peter L. Bartlett, and Jonathan Baxter. Variance reduction techniques for  
 544 gradient estimates in reinforcement learning. In *Proceedings of the 15th International Conference  
 545 on Neural Information Processing Systems: Natural and Synthetic*, NIPS'01, pp. 1507–1514,  
 546 Cambridge, MA, USA, 2001. MIT Press.

547 Daya Guo, Dejian Yang, Haowei Zhang, Junxiao Song, Peiyi Wang, Qihao Zhu, Runxin Xu, Ruoyu  
 548 Zhang, Shirong Ma, Xiao Bi, Xiaokang Zhang, Xingkai Yu, Yu Wu, Z. F. Wu, Zhibin Gou, Zhi-  
 549 hong Shao, Zhuoshu Li, Ziyi Gao, Aixin Liu, Bing Xue, Bingxuan Wang, Bochao Wu, Bei Feng,  
 550 Chengda Lu, Chenggang Zhao, Chengqi Deng, Chong Ruan, Damai Dai, Deli Chen, Dongjie  
 551 Ji, Erhang Li, Fangyun Lin, Fucong Dai, Fuli Luo, Guangbo Hao, Guanting Chen, Guowei Li,  
 552 H. Zhang, Hanwei Xu, Honghui Ding, Huazuo Gao, Hui Qu, Hui Li, Jianzhong Guo, Jiashi Li,  
 553 Jingchang Chen, Jingyang Yuan, Jinhao Tu, Junjie Qiu, Junlong Li, J. L. Cai, Jiaqi Ni, Jian Liang,  
 554 Jin Chen, Kai Dong, Kai Hu, Kaichao You, Kaige Gao, Kang Guan, Kexin Huang, Kuai Yu, Lean  
 555 Wang, Lecong Zhang, Liang Zhao, Litong Wang, Liyue Zhang, Lei Xu, Leyi Xia, Mingchuan  
 556 Zhang, Minghua Zhang, Minghui Tang, Mingxu Zhou, Meng Li, Miaojun Wang, Mingming  
 557 Li, Ning Tian, Panpan Huang, Peng Zhang, Qiancheng Wang, Qinyu Chen, Qiushi Du, Ruiqi  
 558 Ge, Ruisong Zhang, Ruizhe Pan, Runji Wang, R. J. Chen, R. L. Jin, Ruyi Chen, Shanghao Lu,  
 559 Shangyan Zhou, Shanhua Chen, Shengfeng Ye, Shiyu Wang, Shuiping Yu, Shunfeng Zhou,  
 560 Shuting Pan, S. S. Li, Shuang Zhou, Shaoqing Wu, Tao Yun, Tian Pei, Tianyu Sun, T. Wang,  
 561 Wangding Zeng, Wen Liu, Wenfeng Liang, Wenjun Gao, Wenqin Yu, Wentao Zhang, W. L. Xiao,  
 562 Wei An, Xiaodong Liu, Xiaohan Wang, Xiaokang Chen, Xiaotao Nie, Xin Cheng, Xin Liu, Xin  
 563 Xie, Xingchao Liu, Xinyu Yang, Xinyuan Li, Xuecheng Su, Xuheng Lin, X. Q. Li, Xiangyue Jin,  
 564 Xiaojin Shen, Xiaosha Chen, Xiaowen Sun, Xiaoxiang Wang, Xinnan Song, Xinyi Zhou, Xianzu  
 565 Wang, Xinxia Shan, Y. K. Li, Y. Q. Wang, Y. X. Wei, Yang Zhang, Yanhong Xu, Yao Li, Yao Zhao,  
 566 Yaofeng Sun, Yaohui Wang, Yi Yu, Yichao Zhang, Yifan Shi, Yiliang Xiong, Ying He, Yishi  
 567 Piao, Yisong Wang, Yixuan Tan, Yiyang Ma, Yiyuan Liu, Yongqiang Guo, Yuan Ou, Yuduan  
 568 Wang, Yue Gong, Yuheng Zou, Yujia He, Yunfan Xiong, Yuxiang Luo, Yuxiang You, Yuxuan Liu,  
 569 Yuyang Zhou, Y. X. Zhu, Yanping Huang, Yaohui Li, Yi Zheng, Yuchen Zhu, Yunxian Ma, Ying  
 570 Tang, Yukun Zha, Yuting Yan, Z. Z. Ren, Zehui Ren, Zhangli Sha, Zhe Fu, Zhean Xu, Zhenda  
 571 Xie, Zhengyan Zhang, Zhewen Hao, Zhicheng Ma, Zhigang Yan, Zhiyu Wu, Zihui Gu, Zijia Zhu,  
 572 Zijun Liu, Zilin Li, Ziwei Xie, Ziyang Song, Zizheng Pan, Zhen Huang, Zhipeng Xu, Zhongyu  
 573 Zhang, and Zhen Zhang. Deepseek-r1 incentivizes reasoning in llms through reinforcement learning.  
*Nature*, 645(8081):633–638, 2025. ISSN 1476-4687. doi: 10.1038/s41586-025-09422-z.  
 URL <https://doi.org/10.1038/s41586-025-09422-z>.

574 Chaoqun He, Renjie Luo, Yuzhuo Bai, Shengding Hu, Zhen Leng Thai, Junhao Shen, Jinyi  
 575 Hu, Xu Han, Yujie Huang, Yuxiang Zhang, Jie Liu, Lei Qi, Zhiyuan Liu, and Maosong Sun.  
 576 Olympiadbench: A challenging benchmark for promoting agi with olympiad-level bilingual  
 577 multimodal scientific problems, 2024.

578 Peter Henderson, Riashat Islam, Philip Bachman, Joelle Pineau, Doina Precup, and David Meger.  
 579 Deep reinforcement learning that matters. *Proceedings of the AAAI Conference on Artificial  
 580 Intelligence*, 32(1), Apr. 2018. doi: 10.1609/aaai.v32i1.11694. URL <https://ojs.aaai.org/index.php/AAAI/article/view/11694>.

581

582 Dan Hendrycks, Collin Burns, Saurav Kadavath, Akul Arora, Steven Basart, Eric Tang, Dawn Song,  
 583 and Jacob Steinhardt. Measuring mathematical problem solving with the math dataset. *NeurIPS*,  
 584 2021.

585

586 Ari Holtzman, Jan Buys, Li Du, Maxwell Forbes, and Yejin Choi. The curious case of neural text  
 587 degeneration. In *International Conference on Learning Representations*, 2020. URL <https://openreview.net/forum?id=rygGQyrFvH>.

588

589 Jian Hu, Jason Klein Liu, Haotian Xu, and Wei Shen. Reinforce++: An efficient rlhf algorithm  
 590 with robustness to both prompt and reward models, 2025. URL <https://arxiv.org/abs/2501.03262>.

591

592 Hugging Face. Open r1: A fully open reproduction of deepseek-r1, January 2025. URL <https://github.com/huggingface/open-r1>.

593

594 Arthur Juliani and Jordan T. Ash. A study of plasticity loss in on-policy deep re-  
 595 enforcement learning. In A. Globerson, L. Mackey, D. Belgrave, A. Fan, U. Pa-  
 596 quet, J. Tomczak, and C. Zhang (eds.), *Advances in Neural Information Process-  
 597 ing Systems*, volume 37, pp. 113884–113910. Curran Associates, Inc., 2024. URL  
 598 [https://proceedings.neurips.cc/paper\\_files/paper/2024/file/ce7984e36d58659211a8dc7d5457cd6f-Paper-Conference.pdf](https://proceedings.neurips.cc/paper_files/paper/2024/file/ce7984e36d58659211a8dc7d5457cd6f-Paper-Conference.pdf).

600 Kaiser, Mohammad Babaeizadeh, Piotr Miłos, Błażej Osiński, Roy H Campbell, Konrad  
 601 Czechowski, Dumitru Erhan, Chelsea Finn, Piotr Kozakowski, Sergey Levine, Afroz Mohi-  
 602 uddin, Ryan Sepassi, George Tucker, and Henryk Michalewski. Model based reinforce-  
 603 ment learning for atari. In *International Conference on Learning Representations*, 2020. URL  
 604 <https://openreview.net/forum?id=S1xCPJHtDB>.

606 Sham M. Kakade and John Langford. Approximately optimal approximate reinforce-  
 607 ment learning. In *International Conference on Machine Learning*, 2002. URL <https://api.semanticscholar.org/CorpusID:31442909>.

609 Diederik P Kingma and Jimmy Ba. Adam: A method for stochastic optimization. *International  
 610 Conference on Learning Representations*, 2015. URL <https://arxiv.org/abs/1412.6980>.

612 Timo Klein, Lukas Miklautz, Kevin Sidak, Claudia Plant, and Sebastian Tschiatschek. Plasticity loss  
 613 in deep reinforcement learning: A survey, 2024. URL <https://arxiv.org/abs/2411.04832>.

616 Aitor Lewkowycz, Anders Andreassen, David Dohan, Ethan Dyer, Henryk Michalewski, Vinay Ra-  
 617 masesh, Ambrose Slone, Cem Anil, Imanol Schlag, Theo Gutman-Solo, Yuhuai Wu, Behnam  
 618 Neyshabur, Guy Gur-Ari, and Vedant Misra. Solving quantitative reasoning problems with lan-  
 619 guage models, 2022. URL <https://arxiv.org/abs/2206.14858>.

620 Hunter Lightman, Vineet Kosaraju, Yura Burda, Harri Edwards, Bowen Baker, Teddy Lee, Jan  
 621 Leike, John Schulman, Ilya Sutskever, and Karl Cobbe. Let's verify step by step. *arXiv preprint  
 622 arXiv:2305.20050*, 2023.

624 Zichen Liu, Changyu Chen, Wenjun Li, Penghui Qi, Tianyu Pang, Chao Du, Wee Sun Lee, and Min  
 625 Lin. Understanding r1-zero-like training: A critical perspective. In *2nd AI for Math Workshop @  
 626 ICML 2025*, 2025a. URL <https://openreview.net/forum?id=jIpC1zavzn>.

627 Zichen Liu, Changyu Chen, Wenjun Li, Penghui Qi, Tianyu Pang, Chao Du, Wee Sun Lee, and  
 628 Min Lin. Understanding r1-zero-like training: A critical perspective, 2025b. URL <https://arxiv.org/abs/2503.20783>.

631 Clare Lyle, Mark Rowland, Will Dabney, Marta Kwiatkowska, and Yarin Gal. Learning dynam-  
 632 ics and generalization in deep reinforcement learning. In Kamalika Chaudhuri, Stefanie Jegelka,  
 633 Le Song, Csaba Szepesvari, Gang Niu, and Sivan Sabato (eds.), *Proceedings of the 39th Inter-  
 634 national Conference on Machine Learning*, volume 162 of *Proceedings of Machine Learning  
 635 Research*, pp. 14560–14581. PMLR, 17–23 Jul 2022. URL <https://proceedings.mlr.press/v162/lyle22a.html>.

637 Jincheng Mei, Wesley Chung, Valentin Thomas, Bo Dai, Csaba Szepesvari, and Dale Schu-  
 638 urmans. The role of baselines in policy gradient optimization. In S. Koyejo, S. Mo-  
 639 hamed, A. Agarwal, D. Belgrave, K. Cho, and A. Oh (eds.), *Advances in Neural In-  
 640 formation Processing Systems*, volume 35, pp. 17818–17830. Curran Associates, Inc.,  
 641 2022. URL [https://proceedings.neurips.cc/paper\\_files/paper/2022/file/718d02a76d69686a36eccc8cde3e6a41-Paper-Conference.pdf](https://proceedings.neurips.cc/paper_files/paper/2022/file/718d02a76d69686a36eccc8cde3e6a41-Paper-Conference.pdf).

643 Volodymyr Mnih, Koray Kavukcuoglu, David Silver, Andrei A. Rusu, Joel Veness, Marc G.  
 644 Bellemare, Alex Graves, Martin Riedmiller, Andreas K. Fidjeland, Georg Ostrovski, Stig Pe-  
 645 tersen, Charles Beattie, Amir Sadik, Ioannis Antonoglou, Helen King, Dharshan Kumaran,  
 646 Daan Wierstra, Shane Legg, and Demis Hassabis. Human-level control through deep rein-  
 647 forcement learning. *Nature*, 518(7540):529–533, February 2015. ISSN 00280836. URL  
<http://dx.doi.org/10.1038/nature14236>.

648 Kevin P. Murphy. *Probabilistic Machine Learning: An introduction*. MIT Press, 2022. URL  
 649 <http://probml.github.io/book1>.  
 650

651 OpenAI, :, Aaron Jaech, Adam Kalai, Adam Lerer, Adam Richardson, Ahmed El-Kishky, Aiden  
 652 Low, Alec Helyar, Aleksander Madry, Alex Beutel, Alex Carney, Alex Iftimie, Alex Karpenko,  
 653 Alex Tachard Passos, Alexander Neitz, Alexander Prokofiev, Alexander Wei, Allison Tam, Ally  
 654 Bennett, Ananya Kumar, Andre Saraiva, Andrea Vallone, Andrew Duberstein, Andrew Kondrich,  
 655 Andrey Mishchenko, Andy Applebaum, Angela Jiang, Ashvin Nair, Barret Zoph, Behrooz Ghor-  
 656 bani, Ben Rossen, Benjamin Sokolowsky, Boaz Barak, Bob McGrew, Borys Minaiev, Botaao Hao,  
 657 Bowen Baker, Brandon Houghton, Brandon McKinzie, Brydon Eastman, Camillo Lugaresi, Cary  
 658 Bassin, Cary Hudson, Chak Ming Li, Charles de Bourcy, Chelsea Voss, Chen Shen, Chong Zhang,  
 659 Chris Koch, Chris Orsinger, Christopher Hesse, Claudia Fischer, Clive Chan, Dan Roberts, Daniel  
 660 Kappler, Daniel Levy, Daniel Selsam, David Dohan, David Farhi, David Mely, David Robinson,  
 661 Dimitris Tsipras, Doug Li, Dragos Oprica, Eben Freeman, Eddie Zhang, Edmund Wong, Eliz-  
 662 abeth Proehl, Enoch Cheung, Eric Mitchell, Eric Wallace, Erik Ritter, Evan Mays, Fan Wang,  
 663 Felipe Petroski Such, Filippo Ras, Florencia Leon, Foivos Tsimpourlas, Francis Song, Fred  
 664 von Lohmann, Freddie Sulit, Geoff Salmon, Giambattista Parascandolo, Gildas Chabot, Grace  
 665 Zhao, Greg Brockman, Guillaume Leclerc, Hadi Salman, Haiming Bao, Hao Sheng, Hart An-  
 666 drin, Hessam Bagherinezhad, Hongyu Ren, Hunter Lightman, Hyung Won Chung, Ian Kivlichan,  
 667 Ian O'Connell, Ian Osband, Ignasi Clavera Gilaberte, Ilge Akkaya, Ilya Kostrikov, Ilya Sutskever,  
 668 Irina Kofman, Jakub Pachocki, James Lennon, Jason Wei, Jean Harb, Jerry Twore, Jiacheng Feng,  
 669 Jiahui Yu, Jiayi Weng, Jie Tang, Jieqi Yu, Joaquin Quiñonero Candela, Joe Palermo, Joel Parish,  
 670 Johannes Heidecke, John Hallman, John Rizzo, Jonathan Gordon, Jonathan Uesato, Jonathan  
 671 Ward, Joost Huizinga, Julie Wang, Kai Chen, Kai Xiao, Karan Singhal, Karina Nguyen, Karl  
 672 Cobbe, Katy Shi, Kayla Wood, Kendra Rimbach, Keren Gu-Lemberg, Kevin Liu, Kevin Lu,  
 673 Kevin Stone, Kevin Yu, Lama Ahmad, Lauren Yang, Leo Liu, Leon Maksin, Leyton Ho, Liam  
 674 Fedus, Lilian Weng, Linden Li, Lindsay McCallum, Lindsey Held, Lorenz Kuhn, Lukas Kon-  
 675 draciuk, Lukasz Kaiser, Luke Metz, Madelaine Boyd, Maja Trebacz, Manas Joglekar, Mark Chen,  
 676 Marko Tintor, Mason Meyer, Matt Jones, Matt Kaufer, Max Schwarzer, Meghan Shah, Mehmet  
 677 Yatbaz, Melody Y. Guan, Mengyuan Xu, Mengyuan Yan, Mia Glaese, Mianna Chen, Michael  
 678 Lampe, Michael Malek, Michele Wang, Michelle Fradin, Mike McClay, Mikhail Pavlov, Miles  
 679 Wang, Mingxuan Wang, Mira Murati, Mo Bavarian, Mostafa Rohaninejad, Nat McAleese, Neil  
 680 Chowdhury, Neil Chowdhury, Nick Ryder, Nikolas Tezak, Noam Brown, Ofir Nachum, Oleg  
 681 Boiko, Oleg Murk, Olivia Watkins, Patrick Chao, Paul Ashbourne, Pavel Izmailov, Peter Zhokhov,  
 682 Rachel Dias, Rahul Arora, Randall Lin, Rapha Gontijo Lopes, Raz Gaon, Reah Miyara, Reimar  
 683 Leike, Renny Hwang, Rhythm Garg, Robin Brown, Roshan James, Rui Shu, Ryan Cheu, Ryan  
 684 Greene, Saachi Jain, Sam Altman, Sam Toizer, Sam Toyer, Samuel Miserendino, Sandhini Agar-  
 685 wal, Santiago Hernandez, Sasha Baker, Scott McKinney, Scottie Yan, Shengjia Zhao, Shengli Hu,  
 686 Shibani Santurkar, Shraman Ray Chaudhuri, Shuyuan Zhang, Siyuan Fu, Spencer Papay, Steph  
 687 Lin, Suchir Balaji, Suvansh Sanjeev, Szymon Sidor, Tal Broda, Aidan Clark, Tao Wang, Tay-  
 688 lor Gordon, Ted Sanders, Tejal Patwardhan, Thibault Sottiaux, Thomas Degry, Thomas Dimson,  
 689 Tianhao Zheng, Timur Garipov, Tom Stasi, Trapit Bansal, Trevor Creech, Troy Peterson, Tyna  
 690 Eloundou, Valerie Qi, Vineet Kosaraju, Vinnie Monaco, Vitchyr Pong, Vlad Fomenko, Weiyi  
 691 Zheng, Wenda Zhou, Wes McCabe, Wojciech Zaremba, Yann Dubois, Yinghai Lu, Yining Chen,  
 692 Young Cha, Yu Bai, Yuchen He, Yuchen Zhang, Yunyun Wang, Zheng Shao, and Zhuohan Li.  
 693 Openai o1 system card, 2024. URL <https://arxiv.org/abs/2412.16720>.  
 694

695 Long Ouyang, Jeff Wu, Xu Jiang, Diogo Almeida, Carroll L. Wainwright, Pamela Mishkin, Chong  
 696 Zhang, Sandhini Agarwal, Katarina Slama, Alex Ray, John Schulman, Jacob Hilton, Fraser Kel-  
 697 ton, Luke Miller, Maddie Simens, Amanda Askell, Peter Welinder, Paul Christiano, Jan Leike,  
 698 and Ryan Lowe. Training language models to follow instructions with human feedback. In *Pro-  
 699 ceedings of the 36th International Conference on Neural Information Processing Systems*, NIPS  
 700 '22, Red Hook, NY, USA, 2022. Curran Associates Inc. ISBN 9781713871088.  
 701

702 Razvan Pascanu, Tomas Mikolov, and Yoshua Bengio. On the difficulty of training recurrent neural  
 703 networks. In Sanjoy Dasgupta and David McAllester (eds.), *Proceedings of the 30th International  
 704 Conference on Machine Learning*, volume 28 of *Proceedings of Machine Learning Research*, pp.  
 705 1310–1318, Atlanta, Georgia, USA, 17–19 Jun 2013. PMLR. URL <https://proceedings.mlr.press/v28/pascanu13.html>.

702 Adam Paszke, Sam Gross, Soumith Chintala, Gregory Chanan, Edward Yang, Zachary DeVito,  
 703 Zeming Lin, Alban Desmaison, Luca Antiga, and Adam Lerer. Automatic differentiation in  
 704 pytorch. 2017.

705 Jeffrey Pennington, Samuel Schoenholz, and Surya Ganguli. Resurrecting the sigmoid in  
 706 deep learning through dynamical isometry: theory and practice. In I. Guyon, U. Von  
 707 Luxburg, S. Bengio, H. Wallach, R. Fergus, S. Vishwanathan, and R. Garnett (eds.), *Ad-  
 708 vances in Neural Information Processing Systems*, volume 30. Curran Associates, Inc.,  
 709 2017. URL [https://proceedings.neurips.cc/paper\\_files/paper/2017/  
 710 file/d9fc0cdb67638d50f411432d0d41d0ba-Paper.pdf](https://proceedings.neurips.cc/paper_files/paper/2017/file/d9fc0cdb67638d50f411432d0d41d0ba-Paper.pdf).

711 Qwen, :, An Yang, Baosong Yang, Beichen Zhang, Binyuan Hui, Bo Zheng, Bowen Yu, Chengyuan  
 712 Li, Dayiheng Liu, Fei Huang, Haoran Wei, Huan Lin, Jian Yang, Jianhong Tu, Jianwei Zhang,  
 713 Jianxin Yang, Jiaxi Yang, Jingren Zhou, Junyang Lin, Kai Dang, Keming Lu, Keqin Bao, Kexin  
 714 Yang, Le Yu, Mei Li, Mingfeng Xue, Pei Zhang, Qin Zhu, Rui Men, Runji Lin, Tianhao Li,  
 715 Tianyi Tang, Tingyu Xia, Xingzhang Ren, Xuancheng Ren, Yang Fan, Yang Su, Yichang Zhang,  
 716 Yu Wan, Yuqiong Liu, Zeyu Cui, Zhenru Zhang, and Zihan Qiu. Qwen2.5 technical report, 2025.  
 717 URL <https://arxiv.org/abs/2412.15115>.

718 David Rein, Betty Li Hou, Asa Cooper Stickland, Jackson Petty, Richard Yuanzhe Pang, Julien  
 719 Dirani, Julian Michael, and Samuel R. Bowman. Gpqa: A graduate-level google-proof q&a  
 720 benchmark, 2023. URL <https://arxiv.org/abs/2311.12022>.

721 Nicolas Le Roux, Marc G. Bellemare, Jonathan Lebensold, Arnaud Bergeron, Joshua Greaves, Alex  
 722 Fréchette, Carolyne Pelleter, Eric Thibodeau-Laufer, Sándor Toth, and Sam Work. Tapered off-  
 723 policy reinforce: Stable and efficient reinforcement learning for llms, 2025. URL <https://arxiv.org/abs/2503.14286>.

724 John Schulman, Sergey Levine, Pieter Abbeel, Michael Jordan, and Philipp Moritz. Trust region  
 725 policy optimization. In Francis Bach and David Blei (eds.), *Proceedings of the 32nd International  
 726 Conference on Machine Learning*, volume 37 of *Proceedings of Machine Learning Research*, pp.  
 727 1889–1897, Lille, France, 07–09 Jul 2015. PMLR. URL [https://proceedings.mlr.  
 728 press/v37/schulman15.html](https://proceedings.mlr.press/v37/schulman15.html).

729 John Schulman, Filip Wolski, Prafulla Dhariwal, Alec Radford, and Oleg Klimov. Proximal policy  
 730 optimization algorithms, 2017. URL <https://arxiv.org/abs/1707.06347>.

731 Amrith Setlur, Nived Rajaraman, Sergey Levine, and Aviral Kumar. Scaling test-time compute with-  
 732 out verification or rl is suboptimal, 2025. URL <https://arxiv.org/abs/2502.12118>.

733 Zhihong Shao, Peiyi Wang, Qihao Zhu, Runxin Xu, Junxiao Song, Xiao Bi, Haowei Zhang,  
 734 Mingchuan Zhang, Y. K. Li, Y. Wu, and Daya Guo. Deepseekmath: Pushing the limits of mathe-  
 735 matical reasoning in open language models, 2024. URL <https://arxiv.org/abs/2402.03300>.

736 Guangming Sheng, Chi Zhang, Zilingfeng Ye, Xibin Wu, Wang Zhang, Ru Zhang, Yanghua Peng,  
 737 Haibin Lin, and Chuan Wu. Hybridflow: A flexible and efficient rlhf framework. *arXiv preprint  
 738 arXiv: 2409.19256*, 2024.

739 Parshin Shojaee, Aneesh Jain, Sindhu Tipirneni, and Chandan K. Reddy. Execution-based code gen-  
 740 eration using deep reinforcement learning. *Transactions on Machine Learning Research*, 2023.  
 741 ISSN 2835-8856. URL <https://openreview.net/forum?id=0XBuaxqEcG>.

742 Ghada Sokar, Rishabh Agarwal, Pablo Samuel Castro, and Utku Evci. The dormant neuron phe-  
 743 nomenon in deep reinforcement learning. In Andreas Krause, Emma Brunskill, Kyunghyun Cho,  
 744 Barbara Engelhardt, Sivan Sabato, and Jonathan Scarlett (eds.), *Proceedings of the 40th Inter-  
 745 national Conference on Machine Learning*, volume 202 of *Proceedings of Machine Learning  
 746 Research*, pp. 32145–32168. PMLR, 23–29 Jul 2023. URL [https://proceedings.mlr.press/v202/sokar23a.html](https://proceedings.mlr.<br/>
  747 press/v202/sokar23a.html).

748 Nisan Stiennon, Long Ouyang, Jeffrey Wu, Daniel Ziegler, Ryan Lowe, Chelsea Voss, Alec  
 749 Radford, Dario Amodei, and Paul F Christiano. Learning to summarize with human feed-  
 750 back. In H. Larochelle, M. Ranzato, R. Hadsell, M.F. Balcan, and H. Lin (eds.), *Advances in  
 751 752 753 754 755*

756        *Neural Information Processing Systems*, volume 33, pp. 3008–3021. Curran Associates, Inc.,  
 757        2020. URL [https://proceedings.neurips.cc/paper\\_files/paper/2020/file/1f89885d556929e98d3ef9b86448f951-Paper.pdf](https://proceedings.neurips.cc/paper_files/paper/2020/file/1f89885d556929e98d3ef9b86448f951-Paper.pdf).

759

760        Richard S. Sutton, David McAllester, Satinder Singh, and Yishay Mansour. Policy gradient methods  
 761        for reinforcement learning with function approximation. In *Proceedings of the 13th International  
 762        Conference on Neural Information Processing Systems*, NIPS’99, pp. 1057–1063, Cambridge,  
 763        MA, USA, 1999. MIT Press.

764        Yunhao Tang and Rémi Munos. On a few pitfalls in kl divergence gradient estimation for rl, 2025.  
 765        URL <https://arxiv.org/abs/2506.09477>.

766

767        Kimi Team, Angang Du, Bofei Gao, Bowei Xing, Changjiu Jiang, Cheng Chen, Cheng Li, Chenjun  
 768        Xiao, Chenzhuang Du, Chonghua Liao, Chuning Tang, Congcong Wang, Dehao Zhang, Enming  
 769        Yuan, Enzhe Lu, Fengxiang Tang, Flood Sung, Guangda Wei, Guokun Lai, Haiqing Guo, Han  
 770        Zhu, Hao Ding, Hao Hu, Hao Yang, Hao Zhang, Haotian Yao, Haotian Zhao, Haoyu Lu, Haoze  
 771        Li, Haozhen Yu, Hongcheng Gao, Huabin Zheng, Huan Yuan, Jia Chen, Jianhang Guo, Jianlin  
 772        Su, Jianzhou Wang, Jie Zhao, Jin Zhang, Jingyuan Liu, Junjie Yan, Junyan Wu, Lidong Shi,  
 773        Ling Ye, Longhui Yu, Mengnan Dong, Neo Zhang, Ningchen Ma, Qiwei Pan, Qucheng Gong,  
 774        Shaowei Liu, Shengling Ma, Shupeng Wei, Sihan Cao, Siying Huang, Tao Jiang, Weihao Gao,  
 775        Weimin Xiong, Weiran He, Weixiao Huang, Weixin Xu, Wenhao Wu, Wenyang He, Xianghui  
 776        Wei, Xianqing Jia, Xingzhe Wu, Xinran Xu, Xinxing Zu, Xinyu Zhou, Xuehai Pan, Y. Charles,  
 777        Yang Li, Yangyang Hu, Yangyang Liu, Yanru Chen, Yejie Wang, Yibo Liu, Yidao Qin, Yifeng  
 778        Liu, Ying Yang, Yiping Bao, Yulun Du, Yuxin Wu, Yuzhi Wang, Zaida Zhou, Zhaoji Wang,  
 779        Zhaowei Li, Zhen Zhu, Zheng Zhang, Zhexu Wang, Zhilin Yang, Zhiqi Huang, Zihao Huang,  
 780        Ziyao Xu, Zonghan Yang, and Zongyu Lin. Kimi k1.5: Scaling reinforcement learning with llms,  
 2025. URL <https://arxiv.org/abs/2501.12599>.

781        Sharan Vaswani, Olivier Bachem, Simone Totaro, Robert Müller, Shivam Garg, Matthieu Geist,  
 782        Marlos C. Machado, Pablo Samuel Castro, and Nicolas Le Roux. A general class of surro-  
 783        gate functions for stable and efficient reinforcement learning. In Gustau Camps-Valls, Francisco  
 784        J. R. Ruiz, and Isabel Valera (eds.), *Proceedings of The 25th International Conference on Arti-  
 785        ficial Intelligence and Statistics*, volume 151 of *Proceedings of Machine Learning Research*, pp.  
 786        8619–8649. PMLR, 28–30 Mar 2022. URL <https://proceedings.mlr.press/v151/vaswani22a.html>.

787

788        R. J. Williams. Simple statistical gradient-following algorithms for connectionist reinforcement  
 789        learning. *Machine Learning*, 8:229–256, 1992.

790

791        Thomas Wolf, Lysandre Debut, Victor Sanh, Julien Chaumond, Clement Delangue, Anthony Moi,  
 792        Pierrick Cistac, Tim Rault, Rémi Louf, Morgan Funtowicz, Joe Davison, Sam Shleifer, Patrick  
 793        von Platen, Clara Ma, Yacine Jernite, Julien Plu, Canwen Xu, Teven Le Scao, Sylvain Gugger,  
 794        Mariama Drame, Quentin Lhoest, and Alexander M. Rush. Huggingface’s transformers: State-of-  
 795        the-art natural language processing, 2020. URL <https://arxiv.org/abs/1910.03771>.

796

797        An Yang, Beichen Zhang, Binyuan Hui, Bofei Gao, Bowen Yu, Chengpeng Li, Dayiheng Liu,  
 798        Jianhong Tu, Jingren Zhou, Junyang Lin, Keming Lu, Mingfeng Xue, Runji Lin, Tianyu Liu,  
 799        Xingzhang Ren, and Zhenru Zhang. Qwen2.5-math technical report: Toward mathematical ex-  
 800        pert model via self-improvement, 2024. URL <https://arxiv.org/abs/2409.12122>.

801        Shihui Yang, Chengfeng Dou, Peidong Guo, Kai Lu, Qiang Ju, Fei Deng, and Rihui Xin. Dcpo:  
 802        Dynamic clipping policy optimization, 2025a. URL <https://arxiv.org/abs/2509.02333>.

803

804        Zhihe Yang, Xufang Luo, Zilong Wang, Dongqi Han, Zhiyuan He, Dongsheng Li, and Yunjian  
 805        Xu. Do not let low-probability tokens over-dominate in rl for llms. 2025b. URL <https://arxiv.org/abs/2505.12929>.

806

807        Shunyu Yao, Jeffrey Zhao, Dian Yu, Nan Du, Izhak Shafran, Karthik Narasimhan, and Yuan Cao.  
 808        ReAct: Synergizing reasoning and acting in language models. In *International Conference on  
 809        Learning Representations (ICLR)*, 2023.

810 Qiying Yu, Zheng Zhang, Ruofei Zhu, Yufeng Yuan, Xiaochen Zuo, Yu Yue, Weinan Dai,  
811 Tiantian Fan, Gaohong Liu, Lingjun Liu, Xin Liu, Haibin Lin, Zhiqi Lin, Bole Ma, Guang-  
812 ming Sheng, Yuxuan Tong, Chi Zhang, Mofan Zhang, Wang Zhang, Hang Zhu, Jinhua Zhu,  
813 Jiaze Chen, Jiangjie Chen, Chengyi Wang, Hongli Yu, Yuxuan Song, Xiangpeng Wei, Hao  
814 Zhou, Jingjing Liu, Wei-Ying Ma, Ya-Qin Zhang, Lin Yan, Mu Qiao, Yonghui Wu, and Mingx-  
815 uan Wang. Dapo: An open-source llm reinforcement learning system at scale, 2025. URL  
816 <https://arxiv.org/abs/2503.14476>.

817 Kaiyan Zhang, Yuxin Zuo, Bingxiang He, Youbang Sun, Runze Liu, Che Jiang, Yuchen Fan, Kai  
818 Tian, Guoli Jia, Pengfei Li, Yu Fu, Xingtai Lv, Yuchen Zhang, Sihang Zeng, Shang Qu, Haozhan  
819 Li, Shijie Wang, Yuru Wang, Xinwei Long, Fangfu Liu, Xiang Xu, Jiaze Ma, Xuekai Zhu, Ermo  
820 Hua, Yihao Liu, Zonglin Li, Huayu Chen, Xiaoye Qu, Yafu Li, Weize Chen, Zhenzhao Yuan,  
821 Junqi Gao, Dong Li, Zhiyuan Ma, Ganqu Cui, Zhiyuan Liu, Biqing Qi, Ning Ding, and Bowen  
822 Zhou. A survey of reinforcement learning for large reasoning models, 2025. URL <https://arxiv.org/abs/2509.08827>.

823 Daniel M. Ziegler, Nisan Stiennon, Jeffrey Wu, Tom B. Brown, Alec Radford, Dario Amodei, Paul  
824 Christiano, and Geoffrey Irving. Fine-tuning language models from human preferences. *arXiv*  
825 preprint *arXiv:1909.08593*, 2019. URL <https://arxiv.org/abs/1909.08593>.

826  
827  
828  
829  
830  
831  
832  
833  
834  
835  
836  
837  
838  
839  
840  
841  
842  
843  
844  
845  
846  
847  
848  
849  
850  
851  
852  
853  
854  
855  
856  
857  
858  
859  
860  
861  
862  
863

864 A DERIVATION OF THE SECOND-ORDER OPTIMIZATION OBJECTIVE  
865866 In this section, we formally derive the higher-order expansion of the objective function around a  
867 given parameter vector, and present conditions for monotonic improvement. We start by highlighting  
868 a smoothness assumption required for our analysis.869 **Assumption A.1** (Lipschitz continuity of the Hessian). There exists a constant  $L_2 \geq 0$  such that,  
870 for all  $\tau \in [0, 1]$  and all  $\Delta\theta \in \mathbb{R}^d$ ,  
871

872 
$$\|\nabla^2 J(\theta + \tau\Delta\theta) - \nabla^2 J(\theta)\|_{\text{op}} \leq L_2 \tau \|\Delta\theta\|. \quad (14)$$
  
873

874 Assumption A.1 is standard in the analysis of trust-region and cubic-regularized methods, and holds  
875 locally for smooth policy parameterizations.876 **Proposition A.1** (Second-order expansion with integral remainder). *Let  $J : \mathbb{R}^d \rightarrow \mathbb{R}$  be three times  
877 differentiable, and denote  $g \triangleq \nabla J(\theta)$  and  $H \triangleq \nabla^2 J(\theta)$ . For any update direction  $\Delta\theta \in \mathbb{R}^d$ ,  
878 the objective value at the perturbed parameter  $\theta + \Delta\theta$  admits the expansion*  
879

880 
$$J(\theta + \Delta\theta) = J(\theta) + g^\top \Delta\theta + \frac{1}{2} \Delta\theta^\top H \Delta\theta + \int_0^1 (1 - \tau) \Delta\theta^\top (\nabla^2 J(\theta + \tau\Delta\theta) - H) \Delta\theta d\tau. \quad (15)$$
  
881

882 Under Assumption A.1, the following lower-bound holds  
883

884 
$$J(\theta + \Delta\theta) \geq J(\theta) + g^\top \Delta\theta + \frac{1}{2} \Delta\theta^\top H \Delta\theta - \frac{L_2}{6} \|\Delta\theta\|^3. \quad (16)$$
  
885

886 *Proof.* Let  $\phi(\tau) = J(\theta + \tau\Delta\theta)$  for  $\tau \in [0, 1]$ . Then  $\phi'(0) = g^\top \Delta\theta$  and  $\phi''(0) = \Delta\theta^\top H \Delta\theta$ . The  
887 (one-dimensional) Taylor formula with integral remainder gives  
888

889 
$$\phi(1) = \phi(0) + \phi'(0) + \frac{1}{2} \phi''(0) + \int_0^1 (1 - \tau) (\phi''(\tau) - \phi''(0)) d\tau. \quad (17)$$
  
890

891 Since  $\phi''(\tau) - \phi''(0) = \Delta\theta^\top (\nabla^2 J(\theta + \tau\Delta\theta) - H) \Delta\theta$ , we obtain equation 15. Assumption A.1  
892 implies  $|\Delta\theta^\top (\nabla^2 J(\theta + \tau\Delta\theta) - H) \Delta\theta| \leq \|\Delta\theta\|^2 \|\nabla^2 J(\theta + \tau\Delta\theta) - H\|_{\text{op}} \leq L_2 \tau \|\Delta\theta\|^3$ .  
893894 Solving the integral gives  $\int_0^1 (1 - \tau) L_2 \tau d\tau = L_2/6$ . Since this term can be negative, a worst-case  
895 bound yields the inequality 16.  $\square$   
896897  
898  
899  
900  
901  
902  
903  
904  
905  
906  
907  
908  
909  
910  
911  
912  
913  
914  
915  
916  
917

918 **B DERIVATION OF THE POLICY DIVERGENCE QUADRATIC APPROXIMATION**  
919

920 In this section, we formally derive the higher-order expansion of the KL term around a small step  
921  $\Delta\theta$ . Throughout this derivation, we assume standard regularity assumptions hold (e.g., parameter-  
922 independent support, differentiability of  $\log \pi_\theta$ , and dominated convergence so that differentiation  
923 may pass under the expectation). The state averaging distribution  $d_\pi$  is fixed.

924 **Assumption B.1** (Lipschitz continuity of the Fisher curvature). Let  $F(\theta) :=$   
925  $\mathbb{E}_{s \sim d_\pi, a \sim \pi_\theta(\cdot | s)} [\nabla_\theta \log \pi_\theta(a | s) \nabla_\theta \log \pi_\theta(a | s)^\top]$ .

926 There exists a constant  $L_F \geq 0$  such that, for all  $\tau \in [0, 1]$  and all  $\Delta\theta \in \mathbb{R}^d$ ,

927 
$$\|F(\theta + \tau\Delta\theta) - F(\theta)\|_{\text{op}} \leq L_F \tau \|\Delta\theta\|. \quad (18)$$
928

929 Assumption B.1 is analogous to the Assumption A.1 applied to the Fisher geometry.

930 **Lemma B.1** (The grad-log-prob identity). *Under regularity assumptions, the following identity holds:*

931 
$$\mathbb{E}_{s \sim d_\pi, a \sim \pi_\theta(\cdot | s)} [\nabla_\theta \log \pi_\theta(a | s)] = 0. \quad (19)$$
932

933 *Proof.* Fix  $s$ . By normalization,  $\sum_a \pi_\theta(a | s) = 1$ . Differentiating,  $\sum_a \nabla_\theta \pi_\theta(a | s) = 0$ . Since  
934  $\nabla_\theta \pi_\theta = \pi_\theta \nabla_\theta \log \pi_\theta$ , we obtain

935 
$$\sum_a \pi_\theta(a | s) \nabla_\theta \log \pi_\theta(a | s) = 0, \quad (20)$$
936

937 i.e.  $\mathbb{E}_{a \sim \pi_\theta(\cdot | s)} [\nabla_\theta \log \pi_\theta(a | s)] = 0$ . Averaging over  $s \sim d_\pi$  preserves zero.  $\square$ 

938 **Lemma B.2** (Fisher identity). *Under regularity assumptions, the following identity holds:*

939 
$$-\mathbb{E}[\nabla_\theta^2 \log \pi_\theta(a | s)] = \mathbb{E}[\nabla_\theta \log \pi_\theta(a | s) \nabla_\theta \log \pi_\theta(a | s)^\top] =: F(\theta). \quad (21)$$
940

941 *Proof.* Fix  $s$ . Twice differentiating normalization gives  $\nabla_\theta^2 \sum_a \pi_\theta(a | s) = \sum_a \nabla_\theta^2 \pi_\theta(a | s) = 0$ .  
942 Using  $\nabla_\theta^2 \pi_\theta = \pi_\theta (\nabla_\theta^2 \log \pi_\theta + \nabla_\theta \log \pi_\theta \nabla_\theta \log \pi_\theta^\top)$ , we obtain

943 
$$0 = \sum_a \pi_\theta(a | s) \nabla_\theta^2 \log \pi_\theta(a | s) + \sum_a \pi_\theta(a | s) \nabla_\theta \log \pi_\theta(a | s) \nabla_\theta \log \pi_\theta(a | s)^\top. \quad (22)$$
944

945 Recognizing expectations over  $a \sim \pi_\theta(\cdot | s)$  and multiplying by  $-1$  yields

946 
$$-\mathbb{E}_{a \sim \pi_\theta(\cdot | s)} [\nabla_\theta^2 \log \pi_\theta(a | s)] = \mathbb{E}_{a \sim \pi_\theta(\cdot | s)} [\nabla_\theta \log \pi_\theta(a | s) \nabla_\theta \log \pi_\theta(a | s)^\top]. \quad (23)$$
947

948 Averaging over  $s \sim d_\pi$  gives the result.  $\square$ 

949 **Proposition B.1** (Second-order expansion with integral remainder). *Define the average forward KL  
950 as*

951 
$$\bar{D}_{\text{KL}}(\pi_\theta \| \pi_{\theta+\Delta\theta}) := \mathbb{E}_{s \sim d_\pi} [\text{KL}(\pi_\theta(\cdot | s) \| \pi_{\theta+\Delta\theta}(\cdot | s))]. \quad (24)$$
952

953 *Then, for any update  $\Delta\theta$ ,*

954 
$$\bar{D}_{\text{KL}}(\pi_\theta \| \pi_{\theta+\Delta\theta}) = \frac{1}{2} \Delta\theta^\top F(\theta) \Delta\theta + \int_0^1 (1 - \tau) \Delta\theta^\top (F(\theta + \tau\Delta\theta) - F(\theta)) \Delta\theta d\tau. \quad (25)$$
955

956 *And, under Assumption B.1, the following holds:*

957 
$$\bar{D}_{\text{KL}}(\pi_\theta \| \pi_{\theta+\Delta\theta}) = \frac{1}{2} \Delta\theta^\top F(\theta) \Delta\theta + \mathcal{O}(\|\Delta\theta\|^3). \quad (26)$$
958

959 *Proof.* Let  $\phi(\tau) := \bar{D}_{\text{KL}}(\pi_\theta \| \pi_{\theta+\tau\Delta\theta})$ . By the Taylor expansion with integral remainder,

960 
$$\phi(1) = \phi(0) + \phi'(0) + \frac{1}{2} \phi''(0) + \int_0^1 (1 - \tau) (\phi''(\tau) - \phi''(0)) d\tau. \quad (27)$$
961

972 Then  $\phi(0) = 0$ , and  $\phi'(\tau) = -\mathbb{E}[\nabla_{\theta} \log \pi_{\theta+\tau\Delta\theta}(a \mid s)]^\top \Delta\theta$ , so by Lemma B.1,  $\phi'(0) = 0$ .  
 973 Differentiating again and applying Lemma B.2,  
 974

$$975 \quad \phi''(\tau) = \Delta\theta^\top F(\theta + \tau\Delta\theta)\Delta\theta, \quad \phi''(0) = \Delta\theta^\top F(\theta)\Delta\theta. \quad (28)$$

977 Substituting the evaluated terms yields the expansion.  
 978

979 Finally, Assumption B.1 implies

$$980 \quad |\Delta\theta^\top (F(\theta + \tau\Delta\theta) - F(\theta))\Delta\theta| \leq L_F \tau \|\Delta\theta\|^3. \quad (29)$$

982 Integrating  $\int_0^1 (1 - \tau)\tau d\tau = 1/6$ , so the remainder term is  $\mathcal{O}(\|\Delta\theta\|^3)$ .  $\square$   
 983

984  
 985  
 986  
 987  
 988  
 989  
 990  
 991  
 992  
 993  
 994  
 995  
 996  
 997  
 998  
 999  
 1000  
 1001  
 1002  
 1003  
 1004  
 1005  
 1006  
 1007  
 1008  
 1009  
 1010  
 1011  
 1012  
 1013  
 1014  
 1015  
 1016  
 1017  
 1018  
 1019  
 1020  
 1021  
 1022  
 1023  
 1024  
 1025

1026 **C DERIVATION OF GRADIENTS AND CURVATURES UNDER LAST-LAYER**  
 1027 **MODEL**  
 1028

1029 In this section, we formally derive the gradient and curvature expressions assuming the last-layer  
 1030 model.  
 1031

1032 **Proposition C.1** (Gradient w.r.t.last-layer model of a softmax policy). *Let us consider a softmax*  
 1033 *policy*  $\pi_{\theta}(a \mid s) = \frac{\exp(f_{\theta}(s, a))}{\sum_{a'} \exp(f_{\theta}(s, a'))}$ . *Let us also denote the pre-softmax layer by*  $f_{\theta}(s_t) =$   
 1034  $W h_{\bar{\theta}}(s_t)$ ,  $W \in \mathbb{R}^{K \times d_i}$ ,  $h_{\bar{\theta}}(s_t) \in \mathbb{R}^{d_i}$ . *Define*  $\psi := \text{vec}(W) \in \mathbb{R}^{Kd}$ , *with*  $\theta = (\bar{\theta}, \psi)$ ,  
 1035  $K = \dim(\mathcal{V})$ . *Then the policy gradient with respect to*  $\psi$  *of the PG objective:*  
 1036

$$1037 \quad 1038 \quad 1039 \quad J(\theta) = \mathbb{E}_{\tau \sim \pi_{\theta}} \left[ \sum_{t=0}^T \gamma^t A(s_t, a_t) \log \pi_{\theta}(a_t \mid s_t) \right] \quad (30)$$

1040 is given by:  
 1041

$$1042 \quad 1043 \quad \tilde{g}(\psi) = \mathbb{E}_{\tau \sim \pi_{\theta}} \left[ \sum_{t=0}^T \gamma^t A(s_t, a_t) (e_a - \pi_{\theta}(s_t)) \otimes h(s_t) \right], \quad (31)$$

1044 where  $e_a \in \mathbb{R}^K$ ,  $K = \dim(\mathcal{V})$ , denotes the one-hot vector of the realized action  $a_t$  at time  $t$  (i.e.,  
 1045  $e_a = e_{a_t}$ ),  $\pi_{\theta}(s_t) \in \mathbb{R}^K$  is the vector of action probabilities at  $s_t$ , and  $\otimes$  denotes the Kronecker  
 1046 product.  
 1047

1048 *Proof.* Starting from the advantage version of Equation 1, the policy gradient with respect to  $\psi$  is  
 1049 given by  
 1050

$$1051 \quad 1052 \quad \tilde{g}(\psi) = \mathbb{E}_{\tau \sim \pi_{\theta}} \left[ \sum_{t=0}^T \gamma^t A(s_t, a_t) \nabla_{\psi} \log \pi_{\theta}(a_t \mid s_t) \right]. \quad (32)$$

1053 With logits  $f(s_t) = Wh_{\bar{\theta}}(s_t)$ , the Jacobian of the log-softmax with respect to  $f(s_t)$  is:  
 1054

$$1055 \quad 1056 \quad \frac{\partial \log \pi_{\theta}(a \mid s)}{\partial f(s_t)} = e_a - \pi_{\theta}(s_t) \in \mathbb{R}^K. \quad (33)$$

1057 Vectorizing  $W$  gives:  
 1058

$$1059 \quad \frac{\partial f(s_t)}{\partial \psi} = I_K \otimes h_{\bar{\theta}}(s_t)^{\top} \in \mathbb{R}^{K \times Kd}. \quad (34)$$

1060 By the chain rule,  
 1061

$$1062 \quad 1063 \quad \nabla_{\psi} \log \pi_{\theta}(a \mid s) = (e_a - \pi_{\theta}(s_t))^{\top} (I_K \otimes h_{\bar{\theta}}(s_t)^{\top}) = (e_a - \pi_{\theta}(s_t)) \otimes h_{\bar{\theta}}(s_t),$$

1064 where we used standard Kronecker product identities to obtain a vector in  $\mathbb{R}^{Kd}$ . Plugging the ex-  
 1065 pression for  $\nabla_{\psi} \log \pi_{\theta}(a_t \mid s_t)$  into Equation 32 yields  
 1066

$$1067 \quad 1068 \quad 1069 \quad \tilde{g}(\psi) = \mathbb{E}_{\tau \sim \pi_{\theta}} \left[ \sum_{t=0}^T \gamma^t A(s_t, a_t) (e_a - \pi_{\theta}(s_t)) \otimes h(s_t) \right]. \quad (35)$$

1070  $\square$   
 1071

1072 **The Hessian of the Objective.** For the Hessian, we start by extending the PG Theorem for Hessians:  
 1073

1074 **Lemma C.1** (Hessian of the Policy Gradient). *Let*  $\pi_{\theta}(a \mid s)$  *be a differentiable stochastic policy*  
 1075 *and consider the discounted policy gradient objective*

$$1076 \quad 1077 \quad 1078 \quad J(\theta) = \mathbb{E}_{\tau \sim \pi_{\theta}} \left[ \sum_{t=0}^T \gamma^t A(s_t, a_t) \log \pi_{\theta}(a_t \mid s_t) \right], \quad (36)$$

1079 where  $A(s_t, a_t)$  is the advantage function at time  $t$ . Then, the Hessian of  $J(\theta)$  is given by

1080  
 1081  
 1082  $\nabla_{\theta}^2 J(\theta) = \mathbb{E}_{\tau \sim \pi_{\theta}} \left[ \sum_{t=0}^T \gamma^t A(s_t, a_t) (\nabla_{\theta} \log \pi_{\theta}(a_t | s_t) \nabla_{\theta} \log \pi_{\theta}(a_t | s_t)^{\top} + \nabla_{\theta}^2 \log \pi_{\theta}(a_t | s_t)) \right].$   
 1083  
 1084  
 1085  
 1086  
 1087

*Proof.* Taking the first derivative of  $J(\theta)$ , we obtain

1088  
 1089  $\nabla_{\theta} J(\theta) = \mathbb{E}_{\tau \sim \pi_{\theta}} \left[ \sum_{t=0}^T \gamma^t A(s_t, a_t) \nabla_{\theta} \log \pi_{\theta}(a_t | s_t) \right].$   
 1090  
 1091  
 1092

Differentiating once more yields

1093  
 1094  $\nabla_{\theta}^2 J(\theta) = \nabla_{\theta} \mathbb{E}_{\tau \sim \pi_{\theta}} \left[ \sum_{t=0}^T \gamma^t A(s_t, a_t) \nabla_{\theta} \log \pi_{\theta}(a_t | s_t) \right].$   
 1095  
 1096  
 1097

Expanding the expectation explicitly over state–action pairs weighted by the discounted state distribution  $d_{\gamma}^{\pi}(s_t)$  gives

1098  
 1099  $\nabla_{\theta}^2 J(\theta) = \sum_s d_{\gamma}^{\pi}(s_t) \sum_a \nabla_{\theta} \left[ \pi_{\theta}(a | s) A(s, a) \nabla_{\theta} \log \pi_{\theta}(a | s) \right].$   
 1100  
 1101

Applying the product rule, we obtain

1102  
 1103  $\nabla_{\theta}^2 J(\theta) = \sum_s d_{\gamma}^{\pi}(s_t) \sum_a \pi_{\theta}(a | s) A(s, a) \left( \nabla_{\theta} \log \pi_{\theta}(a | s) \nabla_{\theta} \log \pi_{\theta}(a | s)^{\top} + \nabla_{\theta}^2 \log \pi_{\theta}(a | s) \right).$   
 1104  
 1105  
 1106

Rewriting in expectation form gives the final result:

1107  
 1108  $\nabla_{\theta}^2 J(\theta) = \mathbb{E}_{\tau \sim \pi_{\theta}} \left[ \sum_{t=0}^T \gamma^t A(s_t, a_t) (\nabla_{\theta} \log \pi_{\theta}(a_t | s_t) \nabla_{\theta} \log \pi_{\theta}(a_t | s_t)^{\top} + \nabla_{\theta}^2 \log \pi_{\theta}(a_t | s_t)) \right].$   
 1109  
 1110  
 1111  
 1112  
 1113

□

Now, we can state the Hessian form under the last-layer model:

1114  
 1115 **Proposition C.2** (Hessian under Last-Layer Model). *Let us consider a softmax policy  $\pi_{\theta}(a | s) = \frac{\exp(f_{\theta}(s, a))}{\sum_{a'} \exp(f_{\theta}(s, a'))}$ . Let us also denote the pre-softmax layer by  $f(s_t) = Wh_{\bar{\theta}}(s_t)$ ,  $W \in \mathbb{R}^{K \times d}$ ,  $h_{\bar{\theta}}(s_t) \in \mathbb{R}^d$ . Define  $\psi := \text{vec}(W) \in \mathbb{R}^{Kd}$ , with  $\theta = (\bar{\theta}, \psi)$ ,  $K = \dim(\mathcal{V})$ . Then, the Hessian of the discounted policy gradient objective*

1116  
 1117  
 1118  
 1119  
 1120  
 1121  $J(\theta) = \mathbb{E}_{\tau \sim \pi_{\theta}} \left[ \sum_{t=0}^T \gamma^t A(s_t, a_t) \log \pi_{\theta}(a_t | s_t) \right]$   
 1122  
 1123

is given by

1124  
 1125  
 1126  $\tilde{H}(\psi) = \nabla_{\psi}^2 J(\theta) = \mathbb{E}_{\tau \sim \pi_{\theta}} \left[ \sum_{t=0}^T \gamma^t A(s, a) \left( (e_a - \pi_{\theta}(s_t))(e_a - \pi_{\theta}(s_t))^{\top} - F(s_t) \right) \otimes h_{\bar{\theta}}(s_t) h_{\bar{\theta}}(s_t)^{\top} \right],$   
 1127  
 1128  
 1129

where  $e_a \in \mathbb{R}^K$  is the one-hot vector of action  $a$ ,  $\pi_{\theta}(s_t) \in \mathbb{R}^K$  is the vector of action probabilities, and  $F(s_t) := \text{diag}(\pi_{\theta}(s_t)) - \pi_{\theta}(s_t) \pi_{\theta}(s_t)^{\top}$  is the Fisher information matrix at state  $s_t$ .

1130  
 1131  
 1132  
 1133

*Proof.* From Proposition C.1,

$\nabla_{\psi} \log \pi_{\theta}(a_t | s_t) = (e_a - \pi_{\theta}(s_t)) \otimes h_{\bar{\theta}}(s_t).$  (45)

Hence, the outer product is

$$\begin{aligned}
\nabla_{\psi} \log \pi_{\theta}(a_t \mid s_t) \nabla_{\psi} \log \pi_{\theta}(a_t \mid s_t)^{\top} &= \\
&= \left( (e_a - \pi_{\theta}(s_t)) \otimes h_{\bar{\theta}}(s_t) \right) \left( (e_a - \pi_{\theta}(s_t)) \otimes h_{\bar{\theta}}(s_t) \right)^{\top} \\
&= (e_a - \pi_{\theta}(s_t)) (e_a - \pi_{\theta}(s_t))^{\top} \otimes h_{\bar{\theta}}(s_t) h_{\bar{\theta}}(s_t)^{\top},
\end{aligned} \tag{46}$$

where we applied the identity  $(u \otimes v)(u \otimes v)^\top = (uu^\top) \otimes (vv^\top)$ . Next, we compute the second derivative. Since  $\nabla_{\boldsymbol{\psi}} \log \pi_{\boldsymbol{\theta}}(a_t | s_t) = (e_a - \pi_{\boldsymbol{\theta}}(s_t)) \otimes h_{\boldsymbol{\theta}}(s_t)$ , it follows that

$$\nabla_{\psi}^2 \log \pi_{\theta}(a_t \mid s_t) = -\nabla_{\psi} \pi_{\theta}(s_t) \otimes h_{\bar{\theta}}(s_t). \quad (47)$$

Using  $\nabla \pi_{\theta}(s_t) = (\text{diag}(\pi_{\theta}(s_t)) - \pi_{\theta}(s_t)\pi_{\theta}(s_t)^\top) \otimes h_{\bar{\theta}}(s_t)$ , we obtain

$$\begin{aligned}
\nabla_{\psi}^2 \log \pi_{\theta}(a_t \mid s_t) &= & (48) \\
&= -(\text{diag}(\pi_{\theta}(s_t)) - \pi_{\theta}(s_t)\pi_{\theta}(s_t)^{\top}) \otimes h_{\bar{\theta}}(s_t)h_{\bar{\theta}}(s_t)^{\top} \\
&= -F(s_t) \otimes h_{\bar{\theta}}(s_t)h_{\bar{\theta}}(s_t)^{\top}. & (49)
\end{aligned}$$

Finally, substituting both terms into the general Hessian expression from Lemma C.1,

$$\nabla_{\psi}^2 J(\psi) = \mathbb{E}_{s, a \sim \pi_{\psi}} \left[ A(s, a) \left( \nabla_{\psi} \log \pi_{\theta}(a_t \mid s_t) \nabla_{\psi} \log \pi_{\theta}(a_t \mid s_t)^{\top} + \nabla_{\psi}^2 \log \pi_{\theta}(a_t \mid s_t) \right) \right],$$

yields:

$$\tilde{H}(\boldsymbol{\psi}) = \nabla_{\boldsymbol{\psi}}^2 J(\theta) = \mathbb{E}_{\tau \sim \pi_{\boldsymbol{\theta}}} \left[ \sum_{t=0}^T \gamma^t A(s, a) \left( (e_a - \pi_{\boldsymbol{\theta}}(s_t))(e_a - \pi_{\boldsymbol{\theta}}(s_t))^{\top} - F(s_t) \right) \otimes h_{\bar{\boldsymbol{\theta}}}(s_t) h_{\bar{\boldsymbol{\theta}}}(s_t)^{\top} \right], \quad (50)$$

**Proposition C.3** (Fisher Information under the Last-Layer Model). *Let us consider a softmax policy  $\pi_\theta(a \mid s) = \frac{\exp(f_\theta(s, a))}{\sum_{a'} \exp(f_\theta(s, a'))}$ . Let us also denote the pre-softmax layer by  $f(s_t) = Wh_{\bar{\theta}}(s_t)$ ,  $W \in \mathbb{R}^{K \times d}$ ,  $h_{\bar{\theta}}(s_t) \in \mathbb{R}^d$ . Define  $\psi := \text{vec}(W) \in \mathbb{R}^{Kd}$ , with  $\theta = (\bar{\theta}, \psi)$ ,  $K = \dim(\mathcal{V})$ . Then, the Fisher information matrix with respect to  $\psi$  is*

$$\tilde{F}(\psi) = \mathbb{E}_{\tau_\theta \sim \pi_\theta} \left[ \left( (e_{a_t} - \pi_\theta(s_t)) (e_{a_t} - \pi_\theta(s_t))^\top \right) \otimes h_{\bar{a}}(s_t) h_{\bar{a}}(s_t)^\top \right]. \quad (51)$$

where  $e_{a_t} \in \mathbb{R}^K$  is the one-hot vector of the realized action  $a_t$ , and  $\pi_\theta(s_t) \in \mathbb{R}^K$  is the vector of action probabilities at state  $s_t$ .

*Proof.* From Proposition C.1,

$$\nabla_{\mathbf{a}^t} \log \pi_{\theta}(a_t \mid s_t) \equiv (e_{a^t} - \pi_{\theta}(s_t)) \otimes h_{\bar{a}}(s_t). \quad (52)$$

Therefore

$$\nabla_{\theta'} \log \pi_{\theta}(a_t | s_t) \nabla_{\theta'} \log \pi_{\theta}(a_t | s_t)^\top = ((e_{\theta'} - \pi_{\theta}(s_t))(e_{\theta'} - \pi_{\theta}(s_t))^\top) \otimes h_{\bar{\theta}}(s_t) h_{\bar{\theta}}(s_t)^\top \quad (53)$$

where the last step follows from the Kronecker identity  $(u \otimes x)(v \otimes x)^\top = (uv^\top) \otimes (xx^\top)$ . Substituting this into the definition of the discounted Fisher information matrix yields the result.  $\square$

## 1188 D DIRECTIONAL CURVATURES COMPUTATION

1190 In this section, we present our mechanisms to compute Hessian and Fisher directional curvatures.

### 1192 D.1 DIRECTIONAL FISHER CURVATURE

1194 For the last-layer parameters  $\psi = \text{vec}(W)$  with  $W \in \mathbb{R}^{K \times d_i}$ ,  $K = \dim(\mathcal{V})$ , denote by  $U :=$   
 1195  $\text{unvec}(\Delta\psi) \in \mathbb{R}^{K \times d_i}$  the corresponding matrix form of the direction. We aim to compute the  
 1196 curvature of the Fisher information matrix along a direction  $\Delta\psi$  in parameter space. Recall the  
 1197 Fisher information matrix under the Last-Layer Model (Equation 9):

$$1199 \tilde{F}(\psi) = \mathbb{E}_{\tau \sim \pi_\theta} [(u_t u_t^\top) \otimes (h_t h_t^\top)], \quad (54)$$

1201 where  $u_t := e_{a_t} - \pi_\theta(s_t) \in \mathbb{R}^K$  is the policy error vector and  $h_t := h_{\bar{\theta}}(s_t) \in \mathbb{R}^{d_i}$  is the feature  
 1202 vector. Using the Kronecker Vector identity  $\text{vec}(X)^\top (A \otimes B) \text{vec}(X) = \text{Tr}(AXBX^\top)$ :

$$1205 \Delta\psi^\top \tilde{F}(\psi) \Delta\psi = \mathbb{E}_\tau [\text{vec}(U)^\top (u_t u_t^\top \otimes h_t h_t^\top) \text{vec}(U)] \quad (55)$$

$$1206 = \mathbb{E}_\tau [\text{Tr}(u_t u_t^\top U h_t h_t^\top U^\top)]. \quad (56)$$

1208 Let  $v_t := Uh_t \in \mathbb{R}^K$ . Then  $\text{Tr}(u_t u_t^\top v_t v_t^\top) = (u_t^\top v_t)^2$ . And we obtain:

$$1210 \Delta\psi^\top \tilde{F}(\psi) \Delta\psi = \mathbb{E}_{\tau \sim \pi_\theta} [(u_t^\top v_t)^2]. \quad (57)$$

1212 We can estimate the Equation above with samples. Given a batch of  $N$  state-action-time samples  
 1213  $\{(s_i, a_i, t_i)\}_{i=1}^N$ , an estimator of the curvature is:

$$1216 \widehat{\Delta\psi^\top \tilde{F} \Delta\psi} = \frac{1}{N} \sum_{i=1}^N (u_i^\top (\widehat{U} h_i))^2, \quad (58)$$

1218 with  $u_i = e_{a_i} - \pi_\theta(s_i)$  and  $h_i = h_{\bar{\theta}}(s_i)$ . In practice,  $\Delta\psi$  itself is typically estimated from data (e.g.,  
 1219 as a stochastic gradient direction), hence not strictly deterministic. Therefore, estimating Equation  
 1220 58 introduces a mild bias as  $u_t$  and  $h_t$  are statistically dependent.

1222 **Cost Analysis.** The computation requires only vector and matrix–vector operations. Per sample,  
 1223 we compute  $Uh_i$  at cost  $\mathcal{O}(Kd)$  and the dot product  $u_i^\top v_i$  at cost  $\mathcal{O}(K)$ , followed by a scalar  
 1224 square. In memory, we only store  $U$  ( $Kd$  parameters) and the per-sample vectors  $u_i$  and  $h_i$ . This is  
 1225 dramatically cheaper than materializing the full Fisher matrix  $\tilde{F} \in \mathbb{R}^{Kd \times Kd}$ , which would require  
 1226  $(Kd)^2$  entries.

### 1228 D.2 DIRECTIONAL HESSIAN CURVATURE

1229 We now consider the curvature of the Hessian along a direction  $\Delta\psi$ . We also assume the same  
 1230 notation as in subsection D.1. Recall the Hessian under the Last-Layer model (Equation 8):

$$1233 \tilde{H}(\psi) = \mathbb{E}_{\tau \sim \pi_\theta} [A(s, a) (u_t u_t^\top - F(s)) \otimes h_{\bar{\theta}}(s) h_t h_t^\top], \quad (59)$$

1235 where  $F(s) = \text{diag}(\pi_\theta(s)) - \pi_\theta(s) \pi_\theta(s)^\top$  is the Fisher matrix at state  $s$ ,  $u_t := e_{a_t} - \pi_\theta(s_t) \in \mathbb{R}^K$   
 1236 is the policy error vector and  $h_t := h_{\bar{\theta}}(s_t) \in \mathbb{R}^{d_i}$  is the feature vector.

1237 The directional curvature along  $\Delta\psi$  is

$$1240 \Delta\psi^\top \tilde{H}(\psi) \Delta\psi = \mathbb{E}_\tau \left[ \sum_{t=0}^T \gamma^t A(s_t, a_t) \text{vec}(U)^\top ((u_t u_t^\top - F(s_t)) \otimes h_t h_t^\top) \text{vec}(U) \right]. \quad (60)$$

1242 Using the Kronecker–Vector identity  $\text{vec}(X)^\top (A \otimes B) \text{vec}(X) = \text{Tr}(AXBX^\top)$ , we obtain:  
 1243

$$1244 \Delta_\psi^\top \tilde{H}(\psi) \Delta_\psi = \mathbb{E}_\tau \left[ \sum_{t=0}^T \gamma^t A(s_t, a_t) \left( \text{Tr}(u_t u_t^\top U h_t h_t^\top U^\top) - \text{Tr}(F(s_t) U h_t h_t^\top U^\top) \right) \right]. \quad (61)$$

1247 Let  $v_t := Uh_t$ . Then the two traces simplify via  
 1248

$$1249 \text{Tr}(u_t u_t^\top v_t v_t^\top) = (u_t^\top v_t)^2, \quad \text{Tr}(F(s_t) v_t v_t^\top) = v_t^\top F(s_t) v_t,$$

1250 where the first equality uses  $uu^\top vv^\top = (u^\top v)uv^\top$  and  $\text{Tr}(ab^\top) = b^\top a$ , and the second uses  
 1251  $\text{Tr}(Axx^\top) = x^\top Ax$ . Hence,  
 1252

$$1253 \Delta_\psi^\top \tilde{H}(\psi) \Delta_\psi = \mathbb{E}_{\tau \sim \pi_\theta} \left[ \sum_{t=0}^T \gamma^t A(s_t, a_t) \left( (u_t^\top v_t)^2 - v_t^\top F(s_t) v_t \right) \right]. \quad (62)$$

1256 We can estimate the Equation above via samples, noting the same remarks as in subsection D.1. The  
 1257 sample-based estimator is  
 1258

$$1259 \widehat{\Delta_\psi^\top \tilde{H} \Delta_\psi} = \frac{1}{N} \sum_{i=1}^N \gamma^{t_i} A(s_i, a_i) \left( (u_i^\top \hat{v}_i)^2 - \hat{v}_i^\top F(s_i) \hat{v}_i \right), \quad u_i = e_{a_i} - \pi_\theta(s_i), \quad \hat{v}_i = \hat{U} h_{\bar{\theta}}(s_i). \quad (63)$$

1262 **Cost Analysis.** The computation again only involves vectors and matrix–vector operations. Per  
 1263 sample, we compute  $v_t = Uh_t$  at cost  $\mathcal{O}(Kd)$ , then  $(u_t^\top v_t)^2$  at cost  $O(K)$ . The second term  
 1264 requires an analogous computation to the Fisher case in subsection D.1. Hence, the complexity  
 1265 remains  $O(Kd)$  per sample, and the memory cost is linear in  $K$  and  $d$ , avoiding materialization of  
 1266 the full Hessian  $\tilde{H} \in \mathbb{R}^{Kd \times Kd}$ .  
 1267

1268  
 1269  
 1270  
 1271  
 1272  
 1273  
 1274  
 1275  
 1276  
 1277  
 1278  
 1279  
 1280  
 1281  
 1282  
 1283  
 1284  
 1285  
 1286  
 1287  
 1288  
 1289  
 1290  
 1291  
 1292  
 1293  
 1294  
 1295

## 1296 E MONOTONIC POLICY IMPROVEMENT UNDER CAPO

1298 In this section, we formalize the conditions of monotonic improvement under CAPO.

1299 **Assumption E.1** (Bounded curvature and step norms). Let  $\pi_\theta$  be a differentiable policy  
1300 with objective  $J(\theta)$ . Write  $g(\theta) = \nabla_\theta J(\theta)$ ,  $H(\theta) = \nabla_\theta^2 J(\theta)$ , and  $F(\theta) =$   
1301  $\mathbb{E}_{s \sim d_\pi, a \sim \pi_\theta(\cdot|s)} [\nabla_\theta \log \pi_\theta(a|s) \nabla_\theta \log \pi_\theta(a|s)^\top]$ . For  $\Delta\theta \in \mathbb{R}^d$  define the quadratic diagnostics  
1302

$$1303 m_H(\Delta\theta) := g(\theta)^\top \Delta\theta + \frac{1}{2} \Delta\theta^\top H(\theta) \Delta\theta, \quad m_F(\Delta\theta) := \frac{1}{2} \Delta\theta^\top F(\theta) \Delta\theta. \quad (64)$$

1304 Assume:

1306 (i) **(Hessian operator norm bound)**  $\|H(\theta)\|_{\text{op}} \leq M$  for some finite  $M > 0$ , where  
1307  $\|H(\theta)\|_{\text{op}} := \sup_{x \neq 0} \frac{\|H(\theta)x\|}{\|x\|}$ .

1309 (ii) **(Per-candidate step bound)** Every candidate update considered by the algorithm satisfies  
1310  $\|\Delta\theta\| \leq r$  for some  $r > 0$ .

1311 **Remarks.** The step norm bound is standard in practice, since learning rates, clipping, or trust-region  
1312 constraints ensure  $\|\Delta\theta\| \leq r$ . The Hessian bound  $\|H(\theta)\|_{\text{op}} \leq M$  is more restrictive globally, but  
1313 over any compact region of parameter space visited by the algorithm, continuity of  $H(\theta)$  implies a  
1314 finite  $M$ .

1315 **Lemma E.1** (Surrogate–true performance gap). *For any policies  $\pi$  and  $\pi'$ , with  $D_{\text{KL}}(\pi\|\pi')$  the  
1316 average forward KL under  $d_\pi$ ,*

$$1318 J(\pi') \geq L_\pi(\pi') - C \sqrt{D_{\text{KL}}(\pi\|\pi')}, \quad C = \frac{2\gamma}{(1-\gamma)^2} \epsilon \sqrt{2}, \quad (65)$$

1319 where  $|A^\pi(s, a)| \leq \epsilon$  with  $\epsilon$  finite, and  $L_\pi(\pi') := J(\pi) + \mathbb{E}_{s \sim d_\pi, a \sim \pi'(\cdot|s)} [A_\pi(s, a)]$ . Moreover,  
1320 writing  $\pi = \pi_\theta$  and  $\pi' = \pi_{\theta+\Delta\theta}$  for a parameter step  $\Delta\theta$ ,

$$1322 L_{\pi_\theta}(\pi_{\theta'}) - J(\pi_\theta) = g(\theta)^\top \Delta\theta + \frac{1}{2} \Delta\theta^\top H(\theta) \Delta\theta + o(\|\Delta\theta\|^2). \quad (66)$$

1324 *Proof.* The proof of equation 65 is in Achiam et al. (2017). For Equation 66, we define  $\Psi(\theta') :=$   
1325  $L_{\pi_\theta}(\pi_{\theta'})$ . Note that  $\Psi(\theta) = J(\pi_\theta)$ . Now compute the gradient of  $\Psi$  at  $\theta' = \theta$ :

$$1326 \nabla_{\theta'} \Psi(\theta') \Big|_{\theta'=\theta} = \nabla_{\theta'} \mathbb{E}_{s \sim d_\pi, a \sim \pi_{\theta'}(\cdot|s)} [A_\pi(s, a)] \Big|_{\theta'=\theta} \\ 1327 = \mathbb{E}_{s \sim d_\pi, a \sim \pi_\theta} [A_\pi(s, a) \nabla_{\theta'} \log \pi_{\theta'}(a|s)]_{\theta'=\theta} \\ 1329 = \mathbb{E}_{s \sim d_\pi, a \sim \pi} [A_\pi(s, a) \nabla_\theta \log \pi_\theta(a|s)] =: g(\theta), \quad (67)$$

1330 where  $g(\theta)$  is precisely the policy gradient. Differentiate once more:

$$1332 \nabla_{\theta'}^2 \Psi(\theta') \Big|_{\theta'=\theta} = \mathbb{E}_{s \sim d_{\pi_\theta}, a \sim \pi_{\theta'}(\cdot|s)} \left[ A_{\pi_\theta}(s, a) \nabla_{\theta'}^2 \log \pi_{\theta'}(a|s) \right]_{\theta'=\theta} \\ 1333 + \mathbb{E}_{s \sim d_{\pi_\theta}, a \sim \pi_{\theta'}(\cdot|s)} \left[ A_{\pi_\theta}(s, a) \nabla_{\theta'} \log \pi_{\theta'}(a|s) \nabla_{\theta'} \log \pi_{\theta'}(a|s)^\top \right]_{\theta'=\theta} \\ 1335 := H(\theta).$$

1336 By the second-order Taylor expansion,

$$1338 \Psi(\theta + \Delta\theta) = \Psi(\theta) + g(\theta)^\top \Delta\theta + \frac{1}{2} \Delta\theta^\top H(\theta) \Delta\theta + o(\|\Delta\theta\|^2), \quad (68)$$

1340 which is exactly equation 66.  $\square$

1341 **Theorem E.1** (Monotonic improvement under CAPO, restated). *Fix thresholds  $\delta_H > 0$  and  $\delta_F > 0$ .  
1342 Let  $\mathcal{B}$  be a batch of sampled trajectories. Split  $\mathcal{B}$  into disjoint  $N$  subsets  $b_i \subset \mathcal{B}$ , and propose  
1343 candidate subset updates  $\{\Delta\theta_i\}_{i:N}$ . Retain those satisfying:*

$$1344 m_H(\Delta\theta_i) \geq \delta_H = \omega + \frac{1}{2} Mr^2, \quad m_F(\Delta\theta_i) \leq \delta_F, \quad (69)$$

1345 with  $\omega > 0$  and  $M, r$  defined as in Assumption E.1. Let  $\mathcal{B}_{\text{acc}}$  denote the superset of the  $\mathcal{B}$  accepted  
1346 subsets, and define the aggregated update:  $\Delta\theta = \frac{1}{B} \sum_{i \in \mathcal{B}_{\text{acc}}} \Delta\theta_i$ . Then, for two policies  $\pi_\theta$  and  
1347  $\pi_{\theta+\Delta\theta}$ , we obtain:

$$1348 J(\pi_{\theta+\Delta\theta}) - J(\pi_\theta) \geq \omega - C \sqrt{\delta_F}. \quad (70)$$

1349 Thus choosing  $\omega \geq C \sqrt{\delta_F}$  guarantees monotonic improvement:  $J(\pi_{\theta+\Delta\theta}) \geq J(\pi_\theta)$ .

1350 *Proof.* We first establish bounds in the global Fisher and Hessian directional curvatures.  
1351

1352 **Fisher global bound.** Since  $F \succeq 0$ , the quadratic form  $\phi(u) := u^\top F u$  is convex. Thus:

$$1353 \quad 1354 \quad \Delta\theta^\top F \Delta\theta = \left( \frac{1}{B} \sum_{i \in \mathcal{B}_{acc}} \Delta\theta_i \right)^\top F \left( \frac{1}{B} \sum_{i \in \mathcal{B}_{acc}} \Delta\theta_i \right) \leq \frac{1}{B} \sum_{i \in \mathcal{B}_{acc}} \Delta\theta_i^\top F \Delta\theta_i. \quad (71)$$

1355 The inequality above follows from:

$$1356 \quad 1357 \quad \frac{1}{B} \sum_{i \in \mathcal{B}_{acc}} \Delta\theta_i^\top F \Delta\theta_i - \left( \frac{1}{B} \sum_{i \in \mathcal{B}_{acc}} \Delta\theta_i \right)^\top F \left( \frac{1}{B} \sum_{i \in \mathcal{B}_{acc}} \Delta\theta_i \right) \quad (72)$$

$$1359 \quad 1360 \quad = \frac{1}{2B^2} \sum_{i, j \in \mathcal{B}_{acc}} (\Delta\theta_i - \Delta\theta_j)^\top F (\Delta\theta_i - \Delta\theta_j) \geq 0, \quad (73)$$

1361 because  $F \succeq 0$  implies each summand is nonnegative. Hence:

$$1363 \quad 1364 \quad \Delta\theta^\top F \Delta\theta \leq \frac{1}{B} \sum_{i \in \mathcal{B}_{acc}} \Delta\theta_i^\top F \Delta\theta_i \leq \frac{1}{B} \sum_{i \in \mathcal{B}_{acc}} 2m_F(\Delta\theta_i) \leq 2\delta_F. \quad (74)$$

1365 **Hessian global bound.** Expanding  $m_H(\Delta\theta)$ :

$$1366 \quad 1367 \quad m_H(\Delta\theta) = g(\theta)^\top \Delta\theta + \frac{1}{2} \Delta\theta^\top H \Delta\theta \\ 1368 \quad 1369 \quad = g(\theta)^\top \left( \frac{1}{B} \sum_{i \in \mathcal{B}_{acc}} \Delta\theta_i \right) + \frac{1}{2} \left( \frac{1}{B} \sum_{i \in \mathcal{B}_{acc}} \Delta\theta_i \right)^\top H \left( \frac{1}{B} \sum_{j \in \mathcal{B}_{acc}} \Delta\theta_j \right) \\ 1370 \quad 1371 \quad = \frac{1}{B} \sum_{i \in \mathcal{B}_{acc}} g(\theta)^\top \Delta\theta_i + \frac{1}{2B^2} \sum_{i, j \in \mathcal{B}_{acc}} \Delta\theta_i^\top H \Delta\theta_j. \quad (75)$$

1373 We can decompose the quadratic form:

$$1374 \quad 1375 \quad \sum_{i, j \in \mathcal{B}_{acc}} \Delta\theta_i^\top H \Delta\theta_j = \sum_{i \in \mathcal{B}_{acc}} \Delta\theta_i^\top H \Delta\theta_i + \sum_{\substack{i, j \in \mathcal{B}_{acc} \\ i \neq j}} \Delta\theta_i^\top H \Delta\theta_j. \quad (76)$$

1377 Substituting equation 76 into equation 75 and grouping yields

$$1378 \quad 1379 \quad m_H(\Delta\theta) = \frac{1}{B} \sum_{i \in \mathcal{B}_{acc}} m_H(\Delta\theta_i) - \frac{B-1}{2B^2} \sum_{i \in \mathcal{B}_{acc}} \Delta\theta_i^\top H \Delta\theta_i + \frac{1}{2B^2} \sum_{\substack{i, j \in \mathcal{B}_{acc} \\ i \neq j}} \Delta\theta_i^\top H \Delta\theta_j. \quad (77)$$

1381 By the operator norm bound  $\|H\|_{op} \leq M$  and Cauchy–Schwarz,

$$1382 \quad 1383 \quad |\Delta\theta_i^\top H \Delta\theta_j| \leq M \|\Delta\theta_i\| \|\Delta\theta_j\|.$$

1384 Hence, using  $\|\Delta\theta_i\| \leq r$  for all  $i$ ,

$$1385 \quad 1386 \quad \sum_{i \in \mathcal{B}_{acc}} \Delta\theta_i^\top H \Delta\theta_i \leq MBr^2, \quad \sum_{\substack{i, j \in \mathcal{B}_{acc} \\ i \neq j}} \Delta\theta_i^\top H \Delta\theta_j \geq -MB(B-1)r^2. \quad (78)$$

1388 Substituting into equation 77,

$$1389 \quad 1390 \quad m_H(\Delta\theta) \geq \frac{1}{B} \sum_{i \in \mathcal{B}_{acc}} m_H(\Delta\theta_i) - Mr^2 \left( 1 - \frac{1}{B} \right). \quad (79)$$

1391 If each accepted subset satisfies  $m_H(\Delta\theta_i) \geq \omega + Mr^2$ , then averaging gives  
1392  $\frac{1}{B} \sum_{i \in \mathcal{B}_{acc}} m_H(\Delta\theta_i) \geq \omega + Mr^2$ . Plugging into equation 79 yields

$$1394 \quad 1395 \quad m_H(\Delta\theta) \geq \omega + Mr^2 - Mr^2 \left( 1 - \frac{1}{B} \right) = \omega + \frac{Mr^2}{B} \geq \omega. \quad (80)$$

1396 From Equations 65 and 66 of Lemma E.1, we have that:

$$1397 \quad 1398 \quad J(\pi_{\theta+\Delta\theta}) - J(\pi_\theta) \geq \underbrace{g(\theta)^\top \Delta\theta + \frac{1}{2} \Delta\theta^\top H(\theta) \Delta\theta}_{m_H(\Delta\theta)} + o(\|\Delta\theta\|^2) - C \underbrace{\sqrt{D_{KL}(\pi_\theta \|\pi_{\theta+\Delta\theta})}}_{m_F(\Delta\theta) + o(\|\Delta\theta\|^2)} \quad (81)$$

1400 Then, using  $m_F(\Delta\theta) < \delta_F$ ,  $m_H(\Delta\theta) > \omega$ , and assuming the cubic terms negligible,

$$1402 \quad 1403 \quad J(\pi_{\theta+\Delta\theta}) - J(\pi_\theta) \geq \omega - C\sqrt{\delta_F}. \quad (82)$$

1403 Thus choosing  $\omega \geq C\sqrt{\delta_F}$  guarantees monotonic improvement:  $J(\pi_{\theta+\Delta\theta}) \geq J(\pi_\theta)$ .  $\square$

1404 F PSEUDOCODE OF CAPO  
14051406 In this Appendix, we present CAPO’s algorithm.  
14071408 **Algorithm 1:** Curvature-Aware Policy Optimization (CAPO)  
1409

---

**Input** : Policy  $\pi_\theta$ ; batch  $\mathcal{B}$  of sampled trajectories;  
 1410        thresholds  $(\delta_F, \delta_H, \delta_H^{high})$ ;  
 1411        optimizer for the last-layer model (e.g., SGD or Adam).  
**Output:** Updated policy parameters  $\theta$   
 1412

**while** not done **do**

  // Collect data with the current policy  
 1415    Sample a batch  $\mathcal{B} = \{\tau\}_i^N$  of trajectories,  $\tau \sim \pi_\theta$ .  
 1416

**Partition**  $\mathcal{B}$  into disjoint subsets  $\{b_i\}_{i=1}^N$ .  
 1417

**for**  $i = 1, \dots, N$  **in parallel do**

    // Build last-layer meta-model stats on subset  $b_i$   
 1419      Estimate model-based gradient  $\tilde{g}(\psi)$  using Equation 7;  
 1420      Propose  $\Delta\psi_i$  with the optimizer model (e.g.,  $\Delta\psi_i = \alpha \tilde{g}(\psi)$  for SGD, or Adam’s rule)  
 1421      Compute directional curvatures  $\frac{1}{2} \Delta\psi^\top \tilde{H}(\psi) \Delta\psi$ ,  $\Delta\psi^\top \tilde{F}(\psi) \Delta\psi$  as in Appendix D;  
 1422      Compute objective and policy shifts under the last-layer model:  
 1423         $m_H(\Delta\psi) \leftarrow \tilde{g}(\psi)^\top \Delta\psi + \frac{1}{2} \Delta\psi^\top \tilde{H}(\psi) \Delta\psi$ ,  $m_F(\Delta\psi) \leftarrow \frac{1}{2} \Delta\psi^\top \tilde{F}(\psi) \Delta\psi$ .  
 1424      // Local trust-region acceptance test  
 1425      **if**  $\delta_H \leq m_H(\Delta\psi_i) \leq \delta_H^{high}$  **and**  $m_F(\Delta\psi_i) \leq \delta_F$  **then**  
 1426        | Mark subset  $b_i$  as ACCEPT; add to  $\mathcal{B}_{acc}$ .  
 1427      **else**  
 1428        | REJECT  $b_i$ .  
 1429

    // Compute the actual policy update on accepted data  
 1430      **if**  $\mathcal{B}_{acc} \neq \emptyset$  **then**  
 1431        Estimate the objective on accepted samples (e.g., GRPO/PPO surrogate):  
 1432         $\hat{J}(\theta) = \text{pg-objective}(\pi_\theta; \bigcup_{b_i \in \mathcal{B}_{acc}} b_i)$ .  
 1433        // Policy Gradient and parameter update  
 1434         $\theta \leftarrow \theta + \alpha \hat{\nabla}_\theta J$

**return**  $\theta$

---

1436  
1437  
1438  
1439  
1440  
1441  
1442  
1443  
1444  
1445  
1446  
1447  
1448  
1449  
1450  
1451  
1452  
1453  
1454  
1455  
1456  
1457

1458 G REPRODUCIBILITY STATEMENT  
14591460 **Code Release.** To ensure the reproducibility of our research findings, we release our code at  
1461 <https://anonymous.4open.science/r/capo-stable-gradients>. Our imple-  
1462 mentation is based on PyTorch (Paszke et al., 2017) and HuggingFace (Wolf et al., 2020). All baselines  
1463 are available in the released code. We also plan to publish all the experiments logs in WandB  
1464 (Biewald, 2020).1465 **Reproducibility.** We detail our methodology in Sections 4.1 and 5 and our experimental setup in  
1466 Section 6. We provide all hyperparameters used in this work in Appendix J. For all experiments in  
1467 this paper, we report the results over five seeds with standard errors. For the MATH benchmark, we  
1468 report in-training performance every step, while for the TEST benchmark set we evaluate check-  
1469 points every 10 learning steps. For better visualization, we applied smoothing with exponential  
1470 moving average on the curves. All datasets are open-source and available online for academic use.1471 **Compute Resources.** We execute all RL experiments using 4 NVIDIA H100 GPUs. Each seed in  
1472 the regime with aggressive updates takes approximately 4 hours, while the standard regime takes  
1473 approximately one day. Evaluation is done separately in the same hardware, taking approximately  
1474 90 minutes per seed.1475 **LLM Usage Details.** We use LLMs for paper writing to improve grammar, enhance clarity and  
1476 writing flow, and assist with code and mathematical iterations. All outputs generated by the LLMs  
1477 were thoroughly reviewed and verified by the authors to ensure factual accuracy and correctness.1478  
1479  
1480  
1481  
1482  
1483  
1484  
1485  
1486  
1487  
1488  
1489  
1490  
1491  
1492  
1493  
1494  
1495  
1496  
1497  
1498  
1499  
1500  
1501  
1502  
1503  
1504  
1505  
1506  
1507  
1508  
1509  
1510  
1511

1512 **H COMPUTATIONAL COST ANALYSIS**
1513

1514 **Execution Time.** Table 1 reports a breakdown of CAPO’s execution time, including both the model  
1515 estimations and the masking process. The table shows the average time (in seconds) of each operation,  
1516 averaged over all learning iterations, measured on our NVIDIA 4xH100 hardware. The total  
1517 learning iteration time include LLM generations and forward and backward passes. We find that  
1518 CAPO contributes less than 3% of the total step time in a learning iteration, resulting in minimal  
1519 training overhead. Most of the cost arises from computing the Adam gradient and updating its  
1520 moments, since this also requires computing batch gradients on sparse representations. Lastly, the cost  
1521 of computing the mask is minimal, below 0.01 seconds.

1522 **Memory cost.** CAPO uses only volatile GPU memory, since all operations are transient and ten-  
1523 sors are discarded after the masking generation. The main memory usage comes from maintaining  
1524 token-level gradient tensors, which have shape  $(N, T, K, D)$ , corresponding to batch size, com-  
1525 pletion length, top- $K$  probabilities, and the number of parameters in the last-layer model. In our  
1526 experiments, with  $N = 24$ ,  $T = 1024$ ,  $K = 50$ , and  $D = 896$ , this amounts to a volatile memory  
1527 footprint of approximately 2 GB, which is minimal given the scale of LLM training. For compari-  
1528 son, this is significantly less expensive than performing KL regularization, which requires storing  
1529 an additional copy of the LLM in memory for the reference policy.

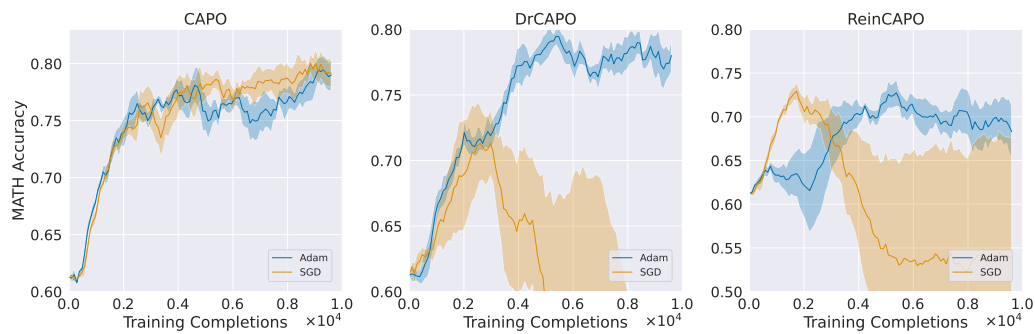
1530

Step	Avg. Time (s)	% of Total
Learning Iteration (Total)	135.84	100.00%
LLM Generations	55.50	40.85%
Total CAPO time	<b>3.99</b>	<b>2.94%</b>
Compute token-level gradients	0.04	0.03%
Compute Adam token gradients	0.51	0.38%
Compute & log $m_H$	0.09	0.07%
Compute & log $m_F$	0.01	0.01%
Update Adam Moments	3.34	2.46%
Compute Hessian Mask	0.00	0.00%
Compute Fisher Mask	0.00	0.00%

1541 Table 1: **Breakdown of the execution time of CAPO.** CAPO contributes less than 3% of the total  
1542 step time, resulting in minimal overhead relative to standard training.

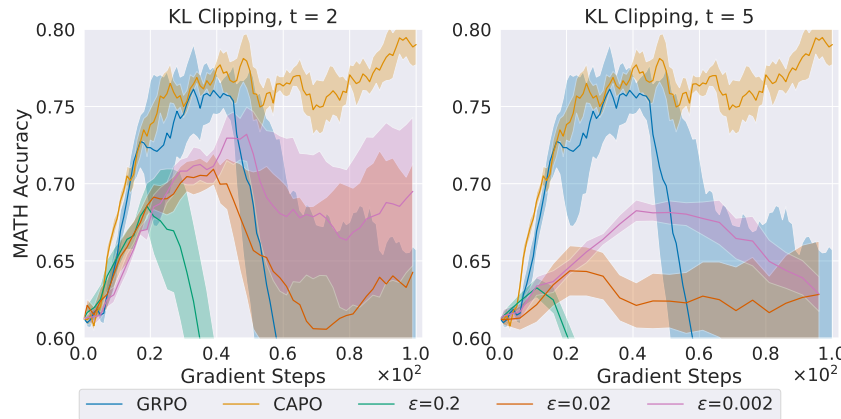
1566 **I ADDITIONAL EXPERIMENTS**  
 1567

1568 **Ablation of the Optimizer Model.** We conducted an ablation study on the impact of the optimizer  
 1569 representation. This choice reflects a trade-off between step accuracy and computational cost: SGD  
 1570 is cheaper, but the LLM policy is optimized with Adam. Figure 6 shows the results on the MATH  
 1571 dataset. For CAPO, representing the optimizer with either SGD or Adam yields similar perfor-  
 1572 mance. However, for Dr.CAPO and ReinCAPO, the SGD variant is insufficient to prevent policy  
 1573 collapse. This suggests that matching the optimizer representation provides a more robust choice  
 1574 across different setups.  
 1575



1576  
 1577 **Figure 6: Ablation study of the optimizer model.** For CAPO, both representations yield similar  
 1578 performance, whereas for Dr.CAPO and ReinCAPO, only the Adam-based representation prevents  
 1579 policy collapse, indicating that matching the optimizer provides a more robust choice across  
 1580 setups.  
 1581

1582 **Is PPO clipping enough to ensure stability?** PPO clipping (Schulman et al., 2017) is a heuristic  
 1583 designed to prevent large updates by clipping the probability ratio between the current policy and  
 1584 the old policy that collected the data. This raises the question of whether clipping alone is sufficient  
 1585 to avoid policy collapse in our LLM setup. We note that clipping is primarily intended to facilitate  
 1586 off-policy updates, whereas our experiments with on-policy data already reveal instability in current  
 1587 RL methods. Nevertheless, we conducted additional experiments using off-policy data reused for  
 1588  $t$  iterations under different clipping ratios. Figure 7 shows results for two setups:  $t = 2$  (minimal  
 1589 off-policy shift) and  $t = 5$  (moderate shift). We find that the standard clipping ratio ( $\epsilon = 0.2$ ) does  
 1590 not prevent collapse. More aggressive ratios alleviate instabilities but reduce performance, likely  
 1591 due to the strong bias introduced in the gradients. This trade-off becomes more pronounced as  $t$   
 1592 increases.  
 1593



1594  
 1595 **Figure 7: Effect of ‘PPO clipping’ on GRPO stability.** Standard clipping ( $\epsilon = 0.2$ ) fails to  
 1596 prevent collapse, while more aggressive ratios improve stability but reduce overall performance,  
 1597 with the trade-off becoming more severe as  $t$  increases.  
 1598

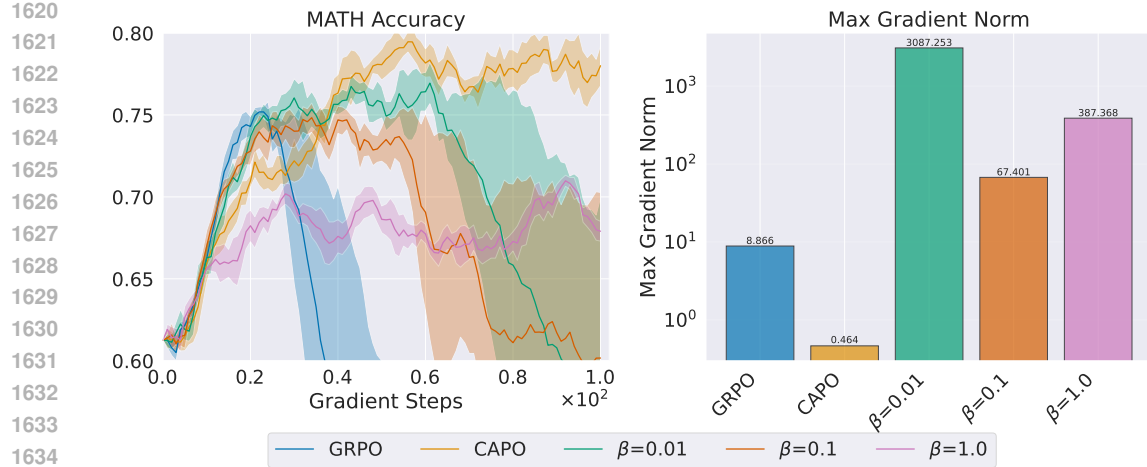


Figure 8: **Effect of KL regularization on GRPO stability.** (Left) Accuracy on the MATH dataset under different levels of KL regularization. Stronger regularization ( $\beta = 1.0$ ) reduces instability but degrades performance. (Right) Maximum gradient norms (before clipping), averaged across seeds. KL regularization produces unbounded gradients that may drive the optimization into unstable regions.

**Is KL regularization enough to ensure stability?** Another common strategy to mitigate instabilities is to add a KL regularizer that penalizes deviations from the base policy (see Equation 3). The rationale is that keeping the policy close to the base model may prevent large distributional shifts, such as those associated with policy collapse. In Figure 8 (left), we test different levels of regularization. We observe a trend similar to clipping: only stronger regularization ( $\beta = 1.0$ ) helps prevent catastrophic updates, but at the cost of performance.

A more fundamental limitation of KL regularization becomes evident when examining its gradient:

$$\nabla_{\theta} \mathcal{D}_{\text{KL}}(\pi_{\theta} \| \pi_{\text{base}}) = \mathbb{E}_{s \sim d^{\pi}, a \sim \pi_{\theta}} \left[ \nabla_{\theta} \log \pi_{\theta}(a | s) \left( \log \frac{\pi_{\theta}(a | s)}{\pi_{\text{base}}(a | s)} + 1 \right) \right]. \quad (83)$$

Differentiating through the KL term introduces a multiplicative log factor, which can produce unbounded gradients. More concretely, as  $\pi_{\text{base}}(a | s) \rightarrow 0$ , the gradient magnitude diverges, effectively “exploding” the LLM policy gradient. We observe this empirically in Figure 8 (right), which shows the maximum gradient norms (before gradient clipping) over training, averaged across seeds. While gradient clipping can reduce the gradient’s magnitude, it does not alter its direction, which may still drive the optimization into unstable regions.

Finally, there are also practical drawbacks to KL regularization. First, it requires storing a full copy of the base model in memory, which has led prior work to abandon the technique (Liu et al., 2025b). Second, differentiating KL estimates as loss functions typically yields biased approximations of the true KL gradient (Tang & Munos, 2025).

1674  
1675  
**J HYPERPARAMETERS**

1676  
1677  
1678  
1679  
1680  
1681  
1682  
In this section, we present the hyperparameters used in our experiments. Table 2 lists the hyperparameters common to all training configurations and algorithms. Table 3 specifies the learning rate and batch size for the conservative and aggressive setups. Finally, Table 4 reports the hyperparameters specific to curvature-aware masking, along with their values for each method. Due to compute budget constraints, we performed manual hyperparameter tuning, primarily searching across different orders of magnitude of both  $\delta_H$  and  $\delta_F$ . For simplicity, we implemented a single symmetric threshold for the Hessian, i.e., rejecting samples outside the interval  $-\delta_H < m_H < \delta_H$ .

Hyperparameter	Value
<i>LLM Generation</i>	
Max Prompt Length	512
Max Completion Length	1024
Num Generations per Prompt	8
Temperature	0.9
<i>Training</i>	
Gradient Steps	100
Warmup Ratio	0.1
Iterations per Batch	1
Optimizer	Adam
LR Scheduler	Cosine
KL $\beta$	0.0

1695  
1696  
Table 2: **Training Hyperparameters.**

Hyperparameter	Standard Setup	Aggressive Setup
Learning Rate	$3 \times 10^{-6}$	$1.5 \times 10^{-5}$
Total Batch Size	1152	96

1700  
1701  
Table 3: **Hyperparameters for the standard (conservative) and aggressive regimes.**

Hyperparameter	CAPO	Dr.CAPO	ReinCAPO
Hessian $\delta_H$	$10^{-2}$	$5 \times 10^{-4}$	$10^{-1}$
Fisher $\delta_F$	$10^{-4}$	$10^{-3}$	$10^{-5}$

1706  
1707  
Table 4: **Curvature-aware masking thresholds for CAPO, Dr.CAPO and ReinCAPO.**

1728 **K MONOTONIC POLICY IMPROVEMENT UNDER CAPO IN THE**  
 1729 **UNDISCOUNTED, FINITE-HORIZON SETTING**  
 1730

1731 Appendix E formalizes the conditions under which CAPO guarantees monotonic improvement in the  
 1732 standard discounted, infinite-horizon setting. Although this formulation is general and aligned with  
 1733 prior RL literature, this section extends the analysis to the undiscounted, finite-horizon setting, which  
 1734 better reflects the LLM reasoning setup and is more consistent with the assumptions underlying  
 1735 practical algorithms such as GRPO.

1736 For this analysis, we consider a finite-horizon Markov decision process (MDP) with horizon  $T \in \mathbb{N}$ ,  
 1737 state space  $\mathcal{S}$ , action space  $\mathcal{A}$ , transition kernel  $P(s' | s, a)$ , reward function  $R : \mathcal{S} \times \mathcal{A} \rightarrow \mathbb{R}$ , and  
 1738 initial state distribution  $\rho_o$ . A (stochastic) policy  $\pi$  is a conditional distribution  $\pi(a | s)$  over actions  
 1739 given states. The return of a policy  $\pi$  is given by:

$$1740 J(\pi) := \mathbb{E}_\pi \left[ \sum_{t=0}^{T-1} R(s_t, a_t) \right]. \quad (84)$$

1741 Furthermore, we define the advantage function as  $A_\pi(s, a) := Q_\pi(s, a) - V_\pi(s)$ . For a second  
 1742 policy  $\pi'$ , we also define the  $\pi'$ -averaged advantage of  $\pi$  at state  $s$ :  $\bar{A}_\pi^{\pi'}(s) := \mathbb{E}_{a \sim \pi'(\cdot | s)}[A_\pi(s, a)]$ .

1743 **Lemma K.1** (Performance Difference Lemma, Finite Horizon,  $\gamma = 1$ ). *Let  $\pi$  and  $\pi'$  be two policies. Then*

$$1744 J(\pi') - J(\pi) = \sum_{t=0}^{T-1} \mathbb{E}_{s \sim d_{\pi',t}} [\bar{A}_\pi^{\pi'}(s)], \quad (85)$$

1745 where  $d_{\pi,t}(s) := \Pr_\pi(s_t = s)$  denotes the time- $t$  state-marginal under  $\pi$ .

1746 *Proof.* We start from the identity  $Q_\pi(s, a) = r(s, a) + \mathbb{E}_{s' \sim P(\cdot | s, a)}[V_\pi(s')]$ . Rearranging,

$$1747 r(s, a) = Q_\pi(s, a) - \mathbb{E}_{s' \sim P(\cdot | s, a)}[V_\pi(s')] = A_\pi(s, a) + V_\pi(s) - \mathbb{E}_{s' \sim P(\cdot | s, a)}[V_\pi(s')]. \quad (86)$$

1748 Consider a trajectory  $(s_0, a_0, \dots, s_{T-1}, a_{T-1})$  generated by policy  $\pi'$ . Then

$$1749 \sum_{t=0}^{T-1} r(s_t, a_t) = \sum_{t=0}^{T-1} (A_\pi(s_t, a_t) + V_\pi(s_t) - \mathbb{E}[V_\pi(s_{t+1}) | s_t, a_t]). \quad (87)$$

1750 Taking expectation under  $\pi'$  and using the law of total expectation,

$$1751 J(\pi') = \mathbb{E}_{\pi'} \left[ \sum_{t=0}^{T-1} A_\pi(s_t, a_t) \right] + \mathbb{E}_{\pi'} \left[ \sum_{t=0}^{T-1} V_\pi(s_t) - V_\pi(s_{t+1}) \right], \quad (88)$$

1752 where  $V_\pi(s_T) := 0$  by definition. The second sum telescopes:

$$1753 \sum_{t=0}^{T-1} V_\pi(s_t) - V_\pi(s_{t+1}) = V_\pi(s_0) - V_\pi(s_T) = V_\pi(s_0). \quad (89)$$

1754 Thus,

$$1755 J(\pi') = \mathbb{E}_{\pi'} \left[ \sum_{t=0}^{T-1} A_\pi(s_t, a_t) \right] + \underbrace{\mathbb{E}_{s_0 \sim \rho_o}[V_\pi(s_0)]}_{J(\pi)}. \quad (90)$$

1756 Therefore,

$$1757 J(\pi') - J(\pi) = \sum_{t=0}^{T-1} \mathbb{E}_{s_t, a_t \sim \pi'}[A_\pi(s_t, a_t)]. \quad (91)$$

1758 We can rewrite each term as

$$1759 \mathbb{E}_{s_t, a_t \sim \pi'}[A_\pi(s_t, a_t)] = \mathbb{E}_{s \sim d_{\pi',t}} [\mathbb{E}_{a \sim \pi'(\cdot | s)}[A_\pi(s, a)]] = \mathbb{E}_{s \sim d_{\pi',t}} [\bar{A}_\pi^{\pi'}(s)], \quad (92)$$

1760 which proves the claimed identity.  $\square$

We now bound the difference between the state marginals  $d_{\pi',t}$  and  $d_{\pi,t}$  in terms of how different the policies are. For  $t \geq 0$ , we first define the policy-induced transition kernels:

$$P_\pi(s' | s) := \sum_a \pi(a | s) P(s' | s, a), \quad P_{\pi'}(s' | s) := \sum_a \pi'(a | s) P(s' | s, a). \quad (93)$$

Then  $d_{\pi,t+1}^\top = d_{\pi,t}^\top P_\pi$  and  $d_{\pi',t+1}^\top = d_{\pi',t}^\top P_{\pi'}$ .

**Lemma K.2** (State-Distribution Shift Bound, Finite Horizon). *Let  $\pi, \pi'$  be two policies with the same initial state distribution  $d_{\pi,0} = d_{\pi',0} = \rho_o$ . Then, for all  $t = 0, \dots, T-1$ ,*

$$\|d_{\pi',t} - d_{\pi,t}\|_1 \leq 2 \sum_{k=0}^{t-1} \mathbb{E}_{s \sim d_{\pi,k}} [D_{\text{TV}}(\pi(\cdot | s), \pi'(\cdot | s))]. \quad (94)$$

*Proof.* Define the difference vector  $\delta_t := d_{\pi',t} - d_{\pi,t}$ . Then:

$$\begin{aligned} \delta_{t+1} &= d_{\pi',t+1} - d_{\pi,t+1} \\ &= d_{\pi',t} P_{\pi'} - d_{\pi,t} P_\pi \\ &= (d_{\pi',t} - d_{\pi,t}) P_{\pi'} + d_{\pi,t} (P_{\pi'} - P_\pi) \\ &= \delta_t P_{\pi'} + d_{\pi,t} (P_{\pi'} - P_\pi). \end{aligned} \quad (95)$$

Since  $P_{\pi'}$  is row-stochastic,  $\|\delta_t P_{\pi'}\|_1 \leq \|\delta_t\|_1$ . Next, we bound the term  $d_{\pi,t} (P_{\pi'} - P_\pi)$ . Let  $w := d_{\pi,t} (P_{\pi'} - P_\pi)$ , so  $w(s') = \sum_s d_{\pi,t}(s) (P_{\pi'}(s' | s) - P_\pi(s' | s))$ . Then:

$$\begin{aligned} \|w\|_1 &= \sum_{s'} |w(s')| = \sum_{s'} \left| \sum_s d_{\pi,t}(s) (P_{\pi'}(s' | s) - P_\pi(s' | s)) \right| \\ &\leq \sum_{s'} \sum_s d_{\pi,t}(s) |P_{\pi'}(s' | s) - P_\pi(s' | s)| \\ &= \sum_s d_{\pi,t}(s) \sum_{s'} |P_{\pi'}(s' | s) - P_\pi(s' | s)| \\ &= \sum_s d_{\pi,t}(s) \|P_{\pi'}(\cdot | s) - P_\pi(\cdot | s)\|_1. \end{aligned} \quad (96)$$

For each fixed  $s$ , using  $P_{\pi'}(s' | s) - P_\pi(s' | s) = \sum_a (\pi'(a | s) - \pi(a | s)) P(s' | s, a)$  and the fact that  $\sum_{s'} P(s' | s, a) = 1$ , we obtain:

$$\begin{aligned} \|P_{\pi'}(\cdot | s) - P_\pi(\cdot | s)\|_1 &= \sum_{s'} \left| \sum_a (\pi'(a | s) - \pi(a | s)) P(s' | s, a) \right| \\ &\leq \sum_{s'} \sum_a |\pi'(a | s) - \pi(a | s)| P(s' | s, a) \\ &= \sum_a |\pi'(a | s) - \pi(a | s)| \\ &= 2D_{\text{TV}}(\pi(\cdot | s), \pi'(\cdot | s)). \end{aligned} \quad (97)$$

Hence  $\|w\|_1 \leq 2 \sum_s d_{\pi,t}(s) D_{\text{TV}}(\pi(\cdot | s), \pi'(\cdot | s))$ . Combining these two bounds and using the triangle inequality,

$$\begin{aligned} \|\delta_{t+1}\|_1 &= \|\delta_t P_{\pi'} + d_{\pi,t} (P_{\pi'} - P_\pi)\|_1 \\ &\leq \|\delta_t P_{\pi'}\|_1 + \|d_{\pi,t} (P_{\pi'} - P_\pi)\|_1 \\ &\leq \|\delta_t\|_1 + 2\alpha_t. \end{aligned} \quad (98)$$

By definition,  $d_{\pi',0} = d_{\pi,0}$ , so  $\delta_0 = 0$  and  $\|\delta_0\|_1 = 0$ . Unrolling the recursion:

$$\|\delta_t\|_1 \leq 2 \sum_{k=0}^{t-1} \mathbb{E}_{s \sim d_{\pi,k}} [D_{\text{TV}}(\pi(\cdot | s), \pi'(\cdot | s))]. \quad (99)$$

□

1836 We now define a surrogate objective based on the reference policy  $\pi$  and the state distributions  $d_{\pi,t}$ .  
 1837  
 1838 **Lemma K.3** (Surrogate–True Performance Gap, Finite Horizon). *For any policies  $\pi$  and  $\pi'$ , with*  
 1839  *$D_{\text{KL}}(\pi\|\pi')$  the average forward KL under  $d_\pi$ ,*

$$1840 \quad J(\pi') \geq L_\pi(\pi') - C \sqrt{D_{\text{KL}}(\pi\|\pi')}, \quad C := T \sqrt{\frac{(T-1)(2T-1)}{3}} \epsilon, \quad (100)$$

1841 where  $|A^\pi(s, a)| \leq \epsilon$  with  $\epsilon$  finite, and  $L_\pi(\pi') := J(\pi) + \sum_{t=0}^{T-1} \mathbb{E}_{s \sim d_{\pi,t}} [\bar{A}_\pi^{\pi'}(s)]$ .

1842  
 1843  
 1844 *Proof.* By Lemma K.1,  $J(\pi') - J(\pi) = \sum_{t=0}^{T-1} \mathbb{E}_{s \sim d_{\pi',t}} [\bar{A}_\pi^{\pi'}(s)]$ . Subtracting the surrogate:

$$1845 \quad J(\pi') - L_\pi(\pi') = \sum_{t=0}^{T-1} \left( \mathbb{E}_{s \sim d_{\pi',t}} \bar{A}_\pi^{\pi'}(s) - \mathbb{E}_{s \sim d_{\pi,t}} \bar{A}_\pi^{\pi'}(s) \right) \\ 1846 \quad = \sum_{t=0}^{T-1} \sum_s (d_{\pi',t}(s) - d_{\pi,t}(s)) \bar{A}_\pi^{\pi'}(s). \quad (101)$$

1852 Taking absolute values and using  $|\bar{A}_\pi^{\pi'}(s)| \leq \epsilon$  and applying Lemma K.2:

$$1853 \quad |J(\pi') - L_\pi(\pi')| \leq \sum_{t=0}^{T-1} \epsilon \|d_{\pi',t} - d_{\pi,t}\|_1 \leq \epsilon \sum_{t=0}^{T-1} 2 \sum_{k=0}^{t-1} \mathbb{E}_{s \sim d_{\pi,k}} [D_{\text{TV}}(\pi(\cdot|s), \pi'(\cdot|s))] \\ 1854 \quad = 2\epsilon \sum_{k=0}^{T-1} \mathbb{E}_{s \sim d_{\pi,k}} [D_{\text{TV}}(\pi(\cdot|s), \pi'(\cdot|s))] \sum_{t=k+1}^{T-1} 1 \\ 1855 \quad = 2\epsilon \sum_{k=0}^{T-1} (T-1-k) \mathbb{E}_{s \sim d_{\pi,k}} [D_{\text{TV}}(\pi(\cdot|s), \pi'(\cdot|s))]. \quad (102)$$

1864 For the KL-based bound, we use Pinsker’s inequality and Jensen’s inequality. For each  $t$ :

$$1865 \quad \mathbb{E}_{s \sim d_{\pi,t}} D_{\text{TV}}(\pi(\cdot|s), \pi'(\cdot|s)) \leq \mathbb{E}_{s \sim d_{\pi,t}} \sqrt{\frac{1}{2} D_{\text{KL}}(\pi(\cdot|s) \parallel \pi'(\cdot|s))} \\ 1866 \quad \leq \sqrt{\frac{1}{2} \mathbb{E}_{s \sim d_{\pi,t}} [D_{\text{KL}}(\pi(\cdot|s) \parallel \pi'(\cdot|s))]} \quad (103)$$

1867 For conciseness, we define  $D_k := D_{\text{KL}}(\pi(\cdot|s) \parallel \pi'(\cdot|s))$ . Then:

$$1868 \quad |J(\pi') - L_\pi(\pi')| \leq 2\epsilon \sum_{k=0}^{T-1} (T-1-k) \sqrt{\frac{1}{2} D_k} = \sqrt{2} \epsilon \sum_{k=0}^{T-1} b_k \sqrt{D_k}, \quad (104)$$

1869 where we have set  $b_k := T-1-k$ . By Cauchy–Schwarz,

$$1870 \quad \sum_{k=0}^{T-1} b_k \sqrt{D_k} \leq \sqrt{\sum_{k=0}^{T-1} b_k^2} \sqrt{\sum_{k=0}^{T-1} D_k}. \quad (105)$$

1871 We note that

$$1872 \quad \sum_{k=0}^{T-1} b_k^2 = \sum_{j=0}^{T-1} j^2 = \frac{(T-1)T(2T-1)}{6}, \quad \sum_{k=0}^{T-1} D_k = T \bar{D}_{\text{KL}}. \quad (106)$$

1873 Therefore

$$1874 \quad |J(\pi') - L_\pi(\pi')| \leq \sqrt{2} \epsilon \sqrt{\frac{(T-1)T(2T-1)}{6}} \sqrt{T \bar{D}_{\text{KL}}} \\ 1875 \quad = T \sqrt{\frac{(T-1)(2T-1)}{3}} \epsilon \sqrt{\bar{D}_{\text{KL}}}. \quad (107)$$

1876  $\square$

1890 The proof of Theorem 5.1 for the finite-horizon setting follows exactly the one in Appendix E, but  
 1891 applying Lemma K.3 instead of Lemma E.1.

1892 **Infinite-Horizon vs. Finite-Horizon bounds.** We highlight that, in both settings, the final guarantee  
 1893 takes the same form  $J(\pi_{\theta+\Delta\theta}) - J(\pi_\theta) \geq \omega - C\sqrt{\delta_F}$ , where  $C = \frac{2\gamma}{(1-\gamma)^2} \epsilon \sqrt{2}$  for the infinite-  
 1894 horizon case, and  $C = T \sqrt{\frac{(T-1)(2T-1)}{3}} \epsilon$  for the finite-horizon case. In both cases, the constant  $C$   
 1895 scales as  $\mathcal{O}(H_{\text{eff}}^2)$ , where  $H_{\text{eff}}$  denotes the effective horizon:  $H_{\text{eff}} = T$  in the finite-horizon setting,  
 1896 and  $H_{\text{eff}} = \frac{1}{1-\gamma}$  in the infinite-horizon setting. Practically, this implies that both bounds are equally  
 1897 tight within their respective regimes.

1898

1899

1900

1901

1902

1903

1904

1905

1906

1907

1908

1909

1910

1911

1912

1913

1914

1915

1916

1917

1918

1919

1920

1921

1922

1923

1924

1925

1926

1927

1928

1929

1930

1931

1932

1933

1934

1935

1936

1937

1938

1939

1940

1941

1942

1943

## 1944 L A CLOSER LOOK AT MODEL ESTIMATES $\hat{m}_F$ AND THE KL POLICY SHIFT

1946 In this section, we analyze the relationship between the model’s estimate of directional Fisher curvature,  $\hat{m}_F$ , and the actual policy shift induced by an update, measured by  $D_{\text{KL}}(\pi_{\theta} \parallel \pi_{\theta+\Delta\theta})$ . Our  
 1947 goals are two-fold: (i) to clarify what CAPO requires from the underlying model in order to approx-  
 1948 imate a trust-region and to assess how well this approximation holds, and (ii) to examine the impact  
 1949 of CAPO’s updates on the true change in policy.  
 1950

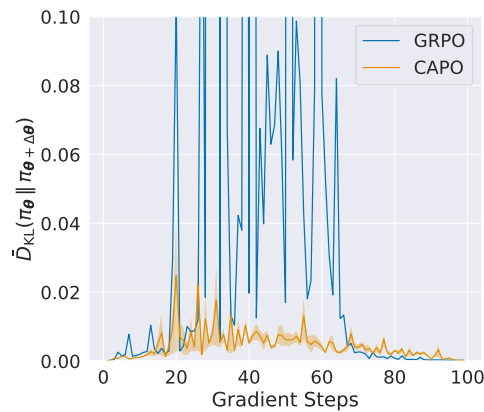
1951 **Does CAPO require a fully calibrated model?** Although well-calibrated estimates are a *sufficient*  
 1952 condition for CAPO’s data-selection mechanism to function effectively, they are not *necessary*. To  
 1953 illustrate this, consider a simple case where the estimated directional Fisher curvature satisfies  $\hat{m}_F =$   
 1954  $\alpha \bar{D}_{\text{KL}}(\pi_{\theta} \parallel \pi_{\theta+\Delta\theta})$ ,  $\alpha > 0$ , where  $\alpha \gg 1$  or  $\alpha \ll 1$ . Such a model is clearly miscalibrated, yet  
 1955 it preserves a strong correlation with the true policy shift. In CAPO, if we aim to enforce the trust-  
 1956 region condition  $\bar{D}_{\text{KL}}(\pi_{\theta}, \parallel \pi_{\theta+\Delta\theta}) < \delta$ , we can simply set the Fisher-threshold to  $\delta_F = \alpha\delta$ ,  
 1957 which recovers the desired constraint. More generally, CAPO only requires that the estimates be  
 1958 *monotonically correlated* with the true policy change, so that large prospective shifts (those most  
 1959 likely to trigger instability or collapse) are reliably identified.

1960 A natural way to evaluate the quality of the model’s estimates is to measure their correlation with the  
 1961 true policy changes. Although we do not have direct access to this quantity, we can estimate it via  
 1962 samples. In particular, the KL divergence can be reliably estimated using a standard Monte Carlo  
 1963 estimator, which has manageable variance and leverages token-level information. We therefore  
 1964 compute these estimates and report the resulting Spearman correlations in the Table 5, where  $\hat{m}_F$   
 1965 is evaluated under both GRPO and CAPO updates at both token and global level. We find that the  
 1966 model estimates exhibit a moderately strong correlation with the actual policy change, indicating  
 1967 a consistent monotonic relationship. Notably, this correlation remains high under both GRPO and  
 1968 CAPO, suggesting that the estimates are meaningful even when they are not used to intervene in the  
 1969 update.

Estimate	$\rho$ (GRPO)	$\rho$ (CAPO)
$\hat{m}_F$ (Token)	0.622	0.459
$\hat{m}_F$ (Global)	0.596	0.498

1973 **Table 5: Spearman correlations  $\rho$  between Fisher directional curvature estimates  $\hat{m}_F$  and the**  
 1974 **estimated policy change  $\bar{D}_{\text{KL}}(\pi_{\theta} \parallel \pi_{\theta+\Delta\theta})$ .** We report correlations for both GRPO and CAPO  
 1975 updates. The results indicate that the estimates  $\hat{m}_F$  maintain a consistent monotonic relationship  
 1976 with the true policy shift across algorithms, reliably identifying the scale of the policy shifts  
 1977

1978 **Ultimately, does CAPO induce a bound on**  
 1979 **the true  $D_{\text{KL}}(\pi_{\theta} \parallel \pi_{\theta+\Delta\theta})$ ?** In Figure 9, we  
 1980 present the policy shifts over the course of  
 1981 training for both algorithms. GRPO frequently  
 1982 presents peaked shifts, which are often associ-  
 1983 ated with unstable or overly aggressive updates.  
 1984 In contrast, CAPO generally maintains stable,  
 1985 small shifts, suggesting that it is effective in  
 1986 practically implementing a trust-region behav-  
 1987 ior throughout training.  
 1988  
 1989  
 1990  
 1991



1992 **Figure 9: Estimated policy KL shifts during**  
 1993 **training.** GRPO exhibits frequent sharp  
 1994 updates, indicative of unstable  
 1995 updates, whereas CAPO maintains consistently  
 1996 small shifts, reflecting its ability to enforce trust-  
 1997 region-like behavior throughout training.

## 1998 2000 2001 2002 2003 2004 2005 2006 2007 2008 2009 2010 2011 2012 2013 2014 2015 2016 2017 2018 2019 2020 2021 2022 2023 2024 2025 2026 2027 2028 2029 2030 2031 2032 2033 2034 2035 2036 2037 2038 2039 2040 2041 2042 2043 2044 2045 2046 2047 2048 2049 2050 2051 M FURTHER QUESTIONS

This Appendix presents additional clarification questions aimed at improving the understanding of the proposed method and experiments. These questions were raised during the peer-review process, and we refer to the OpenReview page for the full discussion.

**What is the effect of token selection in the sample efficiency evaluation?** In Figure 10, we plot the accuracy curves (analogous to Figs. 1 and 2) as a function of the accepted tokens. We observe that these curves closely resemble those obtained when accuracy is plotted against the number of completions. This suggests that the effect of masking on the total number of generated (and accepted) tokens is small, consistent with the rejection rates reported in Figure 5. It also indicates that the learned policies behave similarly in terms of token generation, showing that CAPO improves training sample efficiency without incurring additional inference-time costs.

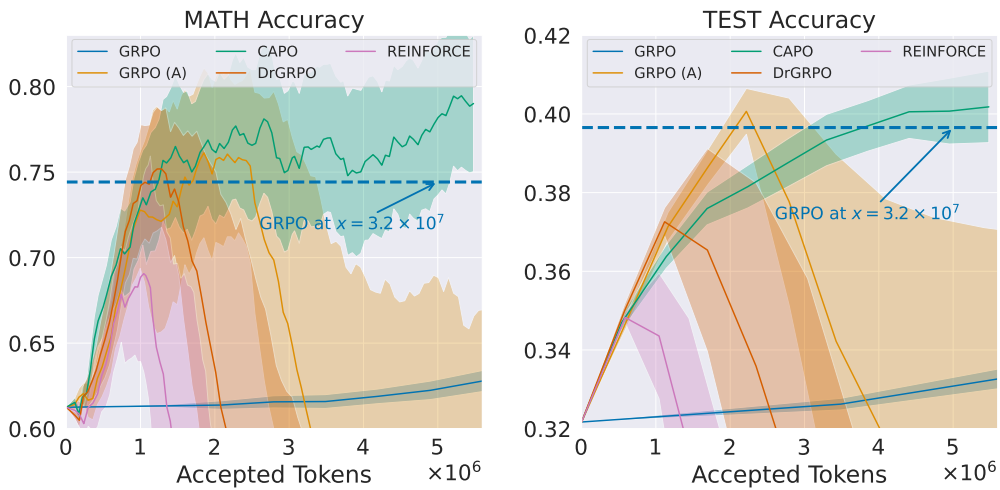


Figure 10: **Sample efficiency curves as a function of the number of accepted tokens.** The trends closely match those obtained when using the number of completions, indicating that masking has minimal impact on token generation and that CAPO improves sample efficiency without added inference cost.

**What are the similarities between CAPO and TRPO? What are the differences?** In terms of similarities, both CAPO and TRPO share the same motivation: devise a conservative optimization procedure that implements a safe optimization region, typically expressed as a KL ball constraint. This idea predates TRPO, with its roots in natural gradient methods from optimization literature Amari (1998); Amari et al. (1995). What both CAPO and TRPO do is to devise practical instantiations of the natural gradient that is suitable for their respective problem settings.

Methodologically, TRPO incorporates *only* the Fisher matrix in its updates, relying on a first-order approximation of the objective. In contrast, CAPO additionally leverages second-order curvature information of the objective through its Hessian, as shown in Equation 5 and further incorporated in the theoretical development in Equation 68. The main difference, however, lies in the implementation, which crucially leads to different scalability properties.

TRPO incorporates the Fisher matrix by employing a Conjugate-Gradient (CG) algorithm to approximate the natural gradient step without fully materializing the Fisher matrix. Then, TRPO employs a line search algorithm to solve the constrained optimization problem. The CG algorithm involves maintaining five vectors of size  $d$  (the gradient, current iterate, the residual, the search direction, and the matrix-vector buffer), where  $d$  is the number of parameters in the policy. While this memory cost is feasible for small deep networks (as usual in traditional Deep RL research), it is prohibitive for LLM scale, where  $d$  is in the billions.

Furthermore, the CG algorithm is iterative, and each iteration costs roughly the same as a backward pass, unless you sacrifice your Fisher matrix estimation by subsampling data. TRPO uses ten itera-

2052 tions. Considering the execution time in our setup (Appendix H), this overhead is also prohibitive.  
2053 Lastly, the line search algorithm requires  $M$  additional forward passes in the whole batch ( $M$  is the  
2054 number of search trials), which is also a substantial cost in our setup (also illustrated in Appendix  
2055 H). Overall, TRPO’s memory and execution costs are prohibitive to LLM scale. CAPO, in contrast,  
2056 leverages the last layer model and the optimizations described in Section 4.1, resulting in much  
2057 lower costs, as evaluated in Table 1 of Appendix H.

2058 In summary, while TRPO and CAPO share the same motivation and draw from the same semi-  
2059 nal work on natural gradients, CAPO offers a formulation that scales to the memory and compute  
2060 demands of LLM policies.

2061

2062

2063

2064

2065

2066

2067

2068

2069

2070

2071

2072

2073

2074

2075

2076

2077

2078

2079

2080

2081

2082

2083

2084

2085

2086

2087

2088

2089

2090

2091

2092

2093

2094

2095

2096

2097

2098

2099

2100

2101

2102

2103

2104

2105